

Article

Distributed Cooperative Tracking Control Strategy for Virtual Coupling Trains: An Event-Triggered Model Predictive Control Approach

Zhongqi Li ^{1,2,*}, Lingyu Zhong ^{1,2}, Hui Yang ^{1,2} and Liang Zhou ^{1,2}

¹ School of Electrical and Automation Engineering, East China Jiaotong University, Nanchang 330013, China; zhonglingyu1206@163.com (L.Z.); yhshuo@163.com (H.Y.); zl971125@163.com (L.Z.)

² State Key Laboratory of Performance Monitoring and Protecting of Rail Transit Infrastructure, East China Jiaotong University, Nanchang 330013, China

* Correspondence: lzq0828@163.com

Abstract: Virtual coupling (VC) technology has received much attention because of its significant advantages in enhancing the railway transport capacity; it achieves efficient train coupling operation through advanced communication technology. However, due to the uncertainty of the operating environment, a stable and effective control system is the key enabler for realization. In this paper, an event-triggered distributed model predictive control (ET-DMPC) method is proposed for the cooperative tracking control of virtual coupling trains (VCTS), considering resource limitations and multiple constraints. Firstly, a distributed model predictive control (DMPC) framework is designed. Based on the established VCTS dynamics model of the dual-leader communication topology, a distributed optimization objective function and safety constraints containing state information of the neighboring train system are constructed. Secondly, due to the limitations of communication and computational resources, the event triggering (ET) mechanism is further introduced, and an ET-DMPC method suitable for VCTS is proposed. The trigger condition of each unit train is designed on the premise of guaranteeing system stability, under which the system can guarantee the input-state stability (ISS), and the recursive feasibility of the system is proven via theoretical analysis. Finally, the VCTS composed of four CRH380A unit trains is used as the control object for simulation experiments, and through two sets of experimental simulation analysis, the effectiveness of the proposed method is verified.

Keywords: virtual coupling train; dual leader topology; collaborative tracking; distributed model predictive control; event trigger conditions; stability



Citation: Li, Z.; Zhong, L.; Yang, H.; Zhou, L. Distributed Cooperative Tracking Control Strategy for Virtual Coupling Trains: An Event-Triggered Model Predictive Control Approach.

Processes **2023**, *11*, 3293. <https://doi.org/10.3390/pr11123293>

Academic Editor: Claudio Urrea

Received: 6 November 2023

Revised: 20 November 2023

Accepted: 21 November 2023

Published: 24 November 2023



Copyright: © 2023 by the authors. Licensee MDPI, Basel, Switzerland. This article is an open access article distributed under the terms and conditions of the Creative Commons Attribution (CC BY) license (<https://creativecommons.org/licenses/by/4.0/>).

1. Introduction

With the increasing demand of passenger and freight transport and the development of wireless communication technology, the study of VC technology of high-speed trains for automatic driving has become the key research direction of the current high-speed railway system [1]. VC technology can not only improve the running efficiency of trains, but also greatly reduces the transport costs through flexible dynamic coupling and decoupling [2]. However, due to the complexity and variability of the operating environment, how to achieve effective control of the VCTS is still an important problem to be solved.

For VCTS, its blocking mode is different from the fixed blocking and traditional mobile blocking, each unit train is tracked with a small spacing less than the braking distance of the train, as shown in Figure 1, by controlling the relative braking distance between the front and rear two unit trains to avoid accidents such as rear-end collisions between unit trains [3]. Therefore, one of the key technologies for the safe operation of VCTS is the safe and efficient tracking control strategy based on the relative distance brake mode (RDBM). Many scholars have carried out relevant research on RDBM-based VCTS operation control.

References [4,5] listed several commonly adopted control methods, including sliding mode control (SMC), machine learning (ML)-based control and model predictive control (MPC). For example, References [6–8] adopted the SMC strategy to control the VCTS in formation considering the effect of external environmental disturbances, and it makes the VCTS track the reference operation state by designing a suitable sliding mode surface. Reference [9] used reinforcement learning (RL) combined with an artificial potential field (APF) for the formation control of VCTS. However, due to the existing track conditions and train performance limitations, the ML-based control is difficult to implement in the actual train operation process, and the stability of the algorithm is not guaranteed. The SMC can track the reference point, but it cannot adjust according to the future operation status of the preceding train. In the actual train operation, the rear train not only has to make adjustments according to the future operation state of the front train to ensure the safety spacing of each unit train, but it also has to ensure that each unit train cannot exceed the track safety speed limit due to the influence of the train braking performance and track conditions. At the same time, in order to satisfy the needs of passenger comfort and energy saving, the train control force should also be limited to a certain range.

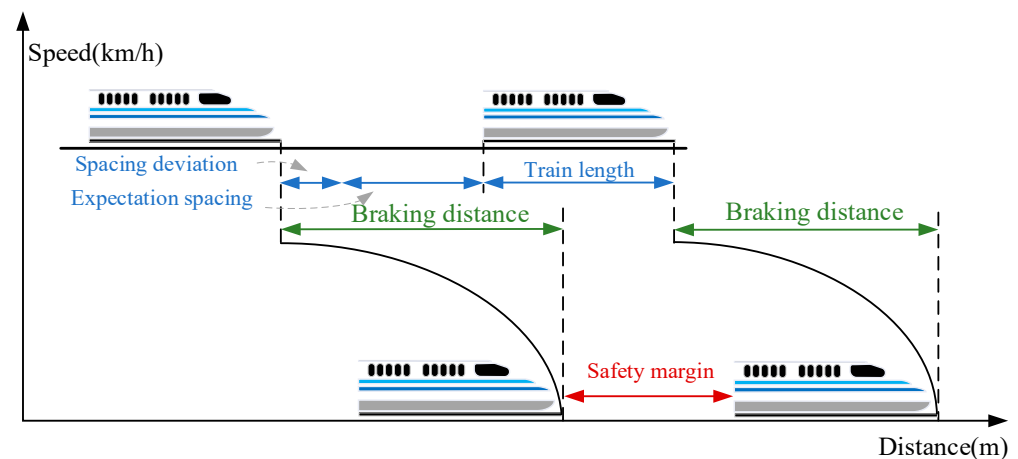


Figure 1. Illustration of VCTS operation mechanism based on RDBM.

Therefore, for the above VCTS operation control problem with constraints, some researchers and scholars have adopted the MPC method with the ability of displaying processing constraints for tracking and controlling the VCTS [10–12]. The method is to calculate the optimal control sequence by solving the performance index function with constraints, and the first control quantity of the sequence is applied to the controlled object, so as to achieve the control objective [13]. For multi-intelligent systems (MASs) such as VCTS, the DMPC strategy is usually adopted, which reduces the computational effort of the controller and improves the reliability of the system compared to the traditional centralized MPC (CMPC) [14]. Under the coverage of the communication network, each controller can interact with its connected controllers and provide control signals to achieve stable system operation. In Reference [15], the authors used DMPC to study the VCTS operation control problem, but the performance index function of the algorithm did not consider the state information of the trains in the topologically connected units, and the design of the control problem was not comprehensive. Reference [16] further considered the state information of the neighboring train system in the performance index function of the DMPC algorithm and achieved a better control effect. Although DMPC is not widely used in the field of VCTS control, it has been studied in the field of vehicle formation [17,18] and unmanned aircraft formation [19,20] control.

However, most of the DMPC algorithms are based on time triggering, i.e., the system periodically solves the optimization problem and transmits the information. However, in real VCTS systems, computational and communication resources are usually very limited. The periodic DMPC causes unnecessary resource consumption. The ET control mecha-

nism is a control method that reduces the resource consumption under the assumption of guaranteeing control performance by executing the appropriate control actions only when the predefined trigger conditions are satisfied. After in-depth research on the ET control mechanism, this method has been successfully applied in many practical systems. Reference [21] combined the ET mechanism with consensus control to study the distributed consistency tracking control problem of MASs. Reference [22] also combined the ET mechanism with adaptive control to track MASs, which reduced the error caused by the ET mechanism and uncertainty perturbation. Reference [23] combined the ET mechanism with distributed fixed-time control to control a multi-terminal DC transmission system. In addition, there are numerous successful cases of combining an ET mechanism with DMPC. Reference [24] proposed a DMPC method for ET multi-intelligent body systems with asynchronous coordination, which uses the state information of neighboring systems to design an ET mechanism and achieves a balance between the consumption of computational and communication resources and the control performance. Reference [25] proposed a DMPC method for adaptive ET, which successfully solved the problems of constraint unsatisfaction and computational resources consumption that occur during the tracking control of MASs. The combination of the ET mechanism and the DMPC algorithm not only retains the advantages of the DMPC algorithm, but it also solves the problem of limited system resources.

Wireless communication technology as one of the bases of VCTS control system implementation; it can ensure that each unit train can receive the state information of its topology connected trains, which can make VCTS in the premise of meeting the safety constraints, to achieve small intervals of co-operative tracking operation, but due to the communication resources usually being limited and the complexity and variability of the communication environment, many feedback controls cannot be achieved in the actual train operation process. Therefore, in order to fill the gap in this field, this paper aims to study a multi-constraint VCTS control system under limited communication and computational resources and proposes a cooperative tracking control algorithm for VCTS based on ET-DMPC.

- (1) Compared with the CMPC in Reference [14], the DMPC method adopted in this paper disperses the computational burden of individual controllers, enhances the cooperative efficiency of formation operation, and improves the control performance of the system, i.e., it greatly reduces the tracking error of each unit train. In order to make the formation more stable, based on Reference [15], we change the topology connection of VCTS and adopt the dual-leader communication topology, and further consider introducing the state information of the neighboring train system into the control performance index function of each unit train. The optimal control quantity is solved for the unit train.
- (2) Compared with the DMPC method used in References [15,16], this paper further introduces the ET condition, that considers the state information of neighboring systems and its own state information, and proposes an ET-DMPC algorithm for cooperative tracking control of VCTS, in order to reduce the impacts of the limited communication and computational resources. For the VCTS control system operating in a fixed communication and computation resource environment, the number of computations and communications using the ET-DMPC method is significantly reduced compared to the DMPC method.
- (3) This paper establishes the theoretical conditions for the feasibility and closed-loop stability of the ET-DMPC algorithm to ensure the theoretical feasibility and stability of the algorithm. The laboratory is equipped with a semi-physical simulation system for high-speed train tracking operation to ensure the practical effectiveness of the algorithm.

The main framework of this paper is as follows: Section 2 introduces the dynamical model of VCTS; Section 3 describes the structural framework of the ET-DMPC algorithm in detail, including the description of the DMPC problem and the design of the ET conditions, and establishes the theoretical conditions to ensure the feasibility of the recursion and

the stability of the closed-loop; and Sections 4 and 5 are the simulation analysis and conclusion, respectively.

2. Dynamic Model of VCTS Operation Process

VCTS is composed of several unit trains, and according to the train dynamics analysis, the dynamics model of the unit train can be expressed as follows [26]:

$$\begin{cases} \dot{s}_i(t) = v_i(t) \\ m_i \dot{v}_i(t) = m_i u_i(t) - (r(v_i(t)) + g(s_i(t))) \end{cases} \quad (1)$$

where $i = 0$ is the index number of the leader train; $i = 1, 2, \dots, N - 1$ are the index numbers of the follower trains; $s_i(t)$ is the actual position of the train i at time t ; $v_i(t)$ is the actual speed of the train i at time t ; m_i is the mass of the train i , in the actual operation of the train, and due to the different train models and loaded goods, the mass of the train is different; $u_i(t)$ is the control input (including traction and braking force) of the train i at time t ; $r(v_i(t)) = c_0 + c_1 v_i(t) + c_2 v_i^2(t)$ is the basic resistance of the train, and c_0, c_1, c_2 are the basic running resistance coefficients, which can be obtained from previous experience. $g(s_i(t))$ is the additional resistance, including the ramp resistance and curve resistance, both of which are related to the location of the train. Because the distance between the two trains of the VCTS is small, this paper assumes that the slope is the same during the train operation.

As shown in Figure 2, this paper adopts the train dual-leader communication topology, through which each unit train can receive the operation information from the two trains in front, such as the position, speed, and control inputs, etc. Under the premise of operating at the same speed, it ensures that there is a safe operation distance between the unit train and the preceding train to avoid a collision. During VCTS operation, the leader train first tracks a given reference speed profile and then transmits its status and control information to the rear train via vehicle-to-vehicle (V2V) communication. Therefore, the state variables of the leader train are defined as follows:

$$\begin{cases} \mathbf{x}_0(t) = [e_0^v(t), 0, e_0^s(t)]^T \\ e_0^v(t) = v_r(t) - v_0(t) \\ e_0^s(t) = s_r(t) - s_0(t) \end{cases} \quad (2)$$

where $v_r(t)$ is the tracking reference velocity at time t ; and $s_r(t)$ is the tracking reference displacement at time t . The state quantity of the follower trains is defined as follows:

$$\begin{cases} \mathbf{x}_i(t) = [x_{i,1}(t), x_{i,2}(t), x_{i,3}(t)]^T = [e_{i,i-1}^v(t), e_{i,i-2}^v(t), e_{i,i-1}^s(t)]^T \\ e_{i,i-1}^v(t) = v_{i-1}(t) - v_i(t) \\ e_{i,i-2}^v(t) = v_{i-2}(t) - v_i(t) \\ e_{i,i-1}^s(t) = s_{i-1}(t) - s_i(t) - d_{i,des} - L_i \end{cases} \quad (3)$$

where $e_{i,i-1}^v(t)$ is the speed deviation between train i and the preceding train $i - 1$ at time t ; $e_{i,i-2}^v(t)$ is the speed deviation between train i and the preceding train $i - 2$ at time t ; $e_{i,i-1}^s(t)$ is the spacing deviation between the actual distance and the desired distance between train i and the preceding train $i - 1$ at time t ; $d_{i,des} = \tau v_{i-1}(t) + d_0$ is the desired distance between train i and the preceding train $i - 1$ to ensure the safe operation at time interval τ ; d_0 is the fixed inter-following distance; and L_i is the length of train i . Therefore, by substituting (1) into (3), it is obtained that

$$\begin{cases} \dot{x}_{i,1}(t) = u_{i-1}(t) - u_i(t) - (2(c_1 + c_2(v_{i-1}(t) + v_i(t)))) / (m_{i-1} + m_i) e_{i,i-1}^v(t) \\ \dot{x}_{i,2}(t) = u_{i-2}(t) - u_i(t) - (2(c_1 + c_2(v_{i-2}(t) + v_i(t)))) / (m_{i-2} + m_i) e_{i,i-2}^v(t) \\ \dot{x}_{i,3}(t) = e_{i,i-1}^v(t) - \tau(u_{i-1}(t) - (c_0 + c_1 v_{i-1}(t) + c_2 v_{i-1}^2(t))) / m_{i-1} \end{cases} \quad (4)$$

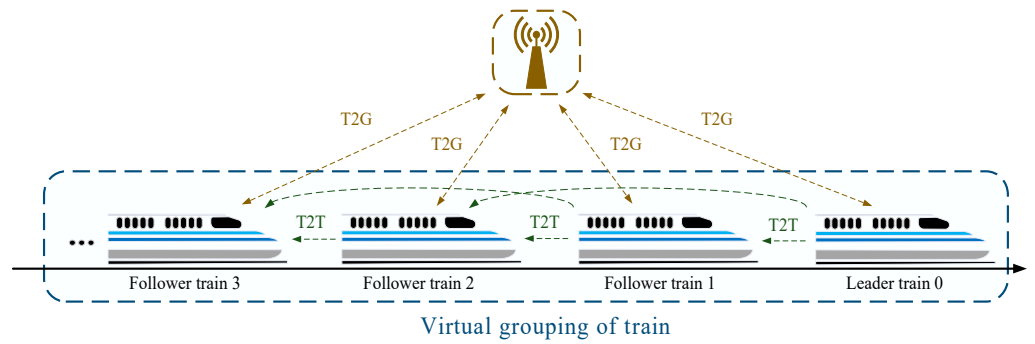


Figure 2. Topology diagram of virtual marshalling train.

In this paper, it is assumed that the mass of each train does not differ much, i.e., m_{i-1} and m_i can be approximated as $(m_{i-1} + m_i)/2$. Since the slope between the two trains is the same, $g(s_i(t))$ can be eliminated. Obviously, in equilibrium, $v_{i-1}(t) + v_i(t) = 2v_r(t)$, and according to Taylor’s formula, $v_i^2(t)$ can be simplified to $v_r^2(t) + 2v_r(t)v_i(t)$. Therefore, the state space model of the VCTS can be expressed as follows:

$$\dot{x}_i(t) = A_i(t)x_i(t) + B_i u_i(t) + C_i(t) \tag{5}$$

In the formula, the matrix coefficients are expressed as follows:

$$A_i(t) = \begin{bmatrix} \frac{2h}{m_{i-1}+m_i} & 0 & 0 \\ 0 & \frac{2h}{m_{i-1}+m_i} & 0 \\ 1 & 0 & 0 \end{bmatrix}, B_i = \begin{bmatrix} -1 \\ -1 \\ 0 \end{bmatrix}, C_i(t) = \begin{bmatrix} u_{i-1}(t) \\ u_{i-2}(t) \\ -\tau(u_{i-1}(t) + \frac{h}{m_{i-1}}v_{i-1}(t) + \frac{c}{m_{i-1}}) \end{bmatrix}$$

where $h = -(c_1 + 2c_2v_r(t))$, $c = -(c_0 - c_2v_r^2(t))$. In the actual train operation process, the train state information is usually transmitted via discrete sampling. Therefore, this paper sets the sampling period as $T_s = 1 s$, and discrete the state space Equation (5) using Eulerian method as

$$x_i(k + 1) = A_{i,s}(k)x_i(k) + B_{i,s}u_i(k) + C_{i,s}(k) \tag{6}$$

where $A_{i,s}(k) = A_i(k)T_s + I$, $B_{i,s} = B_iT_s$, $C_{i,s}(k) = C_i(k)T_s$.

3. Design of ET-DMPC Controller for VCTS

3.1. DMPC Control Problem Design

In order to ensure the safe and reliable operation of the VCTS, it is necessary to introduce state constraints and control constraints to limit the safe operation protection of trains. Due to the influence of train performance and other factors, the train control constraints are as follows:

$$U_{\min}(t) \leq u_i(t) \leq U_{\max}(t) \tag{7}$$

where $U_{\min}(t)$, $U_{\max}(t)$ are the maximum braking deceleration and maximum traction acceleration, respectively. Considering the track conditions and the influence of bad weather, the train speed is limited as follows:

$$0 \leq v_i(t) \leq v_{\lim}(s_i(t)) \tag{8}$$

where $v_{\lim}(s_i(t))$ is the speed limit of train i at operating displacement $s_i(t)$. And in the process of the VCTS operation, in order to exclude the possibility of train tailing, a certain safety distance must be maintained between trains, according to the relative braking curve

of the train, and the safety distance constraints between the neighboring trains can be calculated as:

$$s_{i-1}(t) - s_i(t) - L_i \geq d_{safe} + \max \left\{ \frac{v_{i-1}^2(t)}{2U_{\min}} - \frac{v_i^2(t)}{2U_{\min}}, 0 \right\} \quad (9)$$

where $s_{i-1}(t) - s_i(t) - L_i$ is the actual distance between the two trains; d_{safe} is the braking safety margin; due to the role of the speed limit, it is known that $v_{i-1}(t) + v_i(t) \leq 2v_{\lim}(t)$, and then, Formula (9) can be linearized as follows:

$$s_{i-1}(t) - s_i(t) - L_i \geq d_{safe} \quad (10)$$

$$s_{i-1}(t) - s_i(t) - L_i \geq d_{safe} + \frac{v_{\lim}(t)}{U_{\min}}(v_{i-1}(t) - v_i(t)) \quad (11)$$

When the two trains reach the same speed or the speed of the front train is greater than that of the rear train, the operating spacing of the two trains only needs to satisfy the inequality shown in (10), and when the speed of the front train is less than that of the rear train, the operating spacing of the two trains should satisfy the inequality shown in (11).

In order to facilitate the design of the subsequent VCTS optimal control problem, the following assumptions are given.

Assumption 1 [24]. For the system model (6), given a positive definite symmetric matrix Q , P , R , there exists a constant $\varepsilon > 0$, a positive definite symmetric matrix H and a local state feedback control law $Kx_i + C_i \in \mathbb{U}_i$, such that for any terminal state quantity, there is $x_i \in \mathbb{X}_{if} = \left\{ x_i \in \mathbb{R}^3 : \|(A_{i,s} + B_{i,s}K)x_i\|_H^2 \leq \varepsilon^2 \right\}$, where the terminal state matrix H satisfies $(A_{i,s} + B_{i,s}K)^T H (A_{i,s} + B_{i,s}K) - H + Q + RK^T K \leq 0$, $(A_{i,s} + B_{i,s}K)^T H (A_{i,s} + B_{i,s}K) - H + P \leq 0$.

Remark 1. For the system model (6), when $x_i \in \mathbb{X}_{if}$, according to the local state feedback control law $Kx_i + C_i \in \mathbb{U}_i$, it can be obtained that $x_i(k+1) = (A_{i,s}(k) + B_{i,s}K)x_i(k)$, then $x_i(k+1)^T H x_i(k+1) = ((A_{i,s}(k) + B_{i,s}K)x_i(k))^T H (A_{i,s}(k) + B_{i,s}K)x_i(k) = x_i^T(k)(A_{i,s}(k) + B_{i,s}K)^T H (A_{i,s}(k) + B_{i,s}K)x_i(k)$. And since the terminal matrix H satisfies $(A_{i,s} + B_{i,s}K)^T H (A_{i,s} + B_{i,s}K) - H + Q + RK^T K \leq 0$, it follows that $x_i^T(k)(A_{i,s} + B_{i,s}K)^T H (A_{i,s} + B_{i,s}K)x_i(k) + x_i^T(k)Qx_i(k) + x_i^T(k)RK^T Kx_i(k) \leq x_i^T(k)Hx_i(k) \Rightarrow x_i(k+1)^T H x_i(k+1) \leq x_i^T(k)Hx_i(k)$. Similarly, $x_i(k+1)^T H x_i(k+1) \leq x_i^T(k)Hx_i(k)$ can be obtained from $(A_{i,s} + B_{i,s}K)^T H (A_{i,s} + B_{i,s}K) - H + P \leq 0$. Therefore, the system has bounded convergence, which leads to $x_i \in \mathbb{X}_{if} = \left\{ x_i \in \mathbb{R}^3 : \|(A_{i,s} + B_{i,s}K)x_i\|_H^2 \leq \varepsilon^2 \right\}$. Also for system stability, the terminal matrix H should satisfy $(A_{i,s} + B_{i,s}K)^T H (A_{i,s} + B_{i,s}K) - H + Q + RK^T K \leq 0$ and $(A_{i,s} + B_{i,s}K)^T H (A_{i,s} + B_{i,s}K) - H + P \leq 0$. The proofs can be found in Appendices A and B of the manuscript.

Describe the optimal control problem for the VCTS as follows:

$$\min_{u_i(\cdot|k_i)} J_i(x_i(\cdot|k_i), u_i(\cdot|k_i)) = W_i(x_i(\cdot|k_i), u_i(\cdot|k_i)) + M_i(x_i(\cdot|k_i), u_i(\cdot|k_i)) \quad (12)$$

$$s.t. x_i(k_i + j + 1|k_i) = A_{i,s}(k_i)x_i(k_i + j|k_i) + B_{i,s}u_i(k_i + j|k_i) + C_{i,s}(k_i) \quad (12a)$$

$$x_i(k_i + j|k_i) \in \mathbb{X}_i, j = 1, \dots, N_p - 1 \quad (12b)$$

$$u_i(k_i + j|k_i) \in \mathbb{U}_i, j = 0, \dots, N_p - 1 \quad (12c)$$

$$x_i(k_i + N_p|k_i) \in \mathbb{X}_{if} \quad (12d)$$

In the formula, $W_i(x_i(\cdot|k_i), u_i(\cdot|k_i)), M_i(x_i(\cdot|k_i), u_i(\cdot|k_i))$ are the operation index function and terminal index function, respectively, which are expressed as follows:

$$W_i(x_i(\cdot|k_i), u_i(\cdot|k_i)) = \sum_{j=0}^{N_p-1} (\|x_i(k_i + j|k_i)\|_Q^2 + \|u_i(k_i + j|k_i)\|_R^2) + \|x_i(k_i + j|k_i) - \hat{x}_{i-1}(k_i + j|k_i)\|_P^2 + \|x_i(k_i + j|k_i) - \hat{x}_{i-2}(k_i + j|k_i)\|_P^2 \tag{13}$$

$$M_i(x_i(\cdot|k_i), u_i(\cdot|k_i)) = \|x_i(k_i + N_p|k_i)\|_H^2 + \|x_i(k_i + N_p|k_i) - \hat{x}_{i-1}(k_i + N_p|k_i)\|_H^2 + \|x_i(k_i + N_p|k_i) - \hat{x}_{i-2}(k_i + N_p|k_i)\|_H^2 \tag{14}$$

where N_p is the prediction time domain; $Q, P,$ and R are positive definite symmetric matrices; H is the positive definite weight matrix of the end states that satisfies Assumption 1; $\hat{x}_{i-1}(k_i + j|k_i)$ and $\hat{x}_{i-2}(k_i + j|k_i)$ are the estimated state quantities of train $i - 1$ and train $i - 2$ at time k_i versus time $k_i + j$, respectively; and $x_i(k_i + j|k_i)$ and $u_i(k_i + j|k_i)$ are the predicted state quantities and the control inputs of train i at time k_i versus time $k_i + j$, respectively, which are described as the following constraint sets:

$$u_i(k_i + j|k_i) \in \mathbb{U}_i \triangleq \{u_i \in \mathbb{R} : U_{i,\min}(t) \leq u_i(t) \leq U_{i,\max}(t)\} \tag{15}$$

$$x_i(k_i + j|k_i) \in \mathbb{X}_i \triangleq \{x_i \in \mathbb{R}^3 : \eta_j(x_i) \geq 0, j = 1, \dots, 6\} \tag{16}$$

where

$$\begin{aligned} \eta_1(x_i) &= -G_1x_i + v_{i-1}(t), \\ \eta_2(x_i) &= G_1x_i + v_{\lim} - v_{i-1}(t), \\ \eta_3(x_i) &= -G_2x_i + v_{i-2}(t), \\ \eta_4(x_i) &= G_2x_i + v_{\lim} - v_{i-2}(t), \\ \eta_5(x_i) &= G_3x_i + d_{i,des} - d_{safe}, \\ \eta_6(x_i) &= (G_3 - (v_{\lim}/U_{\min})G_1)x_i + d_{i,des} - d_{safe}. \\ (G_1 &= [1, 0, 0], G_2 = [0, 1, 0], G_3 = [0, 0, 1]) \end{aligned}$$

Remark 2. Due to the fact that VCTS conveys information synchronously, then in this paper, we construct the system estimation state and as follows:

$$\hat{x}_{i-1}(k_i + j|k_i) = \begin{cases} x_{i-1}^*(k_i + j|k_i - 1), j = 0, \dots, N_p - 1 \\ (A_{i-1,s}(k_i - 1) + B_{i-1,s}K)x_{i-1}^*(k_i + N_p - 1|k_i - 1), j = N_p. \end{cases} \tag{17}$$

$$\hat{x}_{i-2}(k_i + j|k_i) = \begin{cases} x_{i-2}^*(k_i + j|k_i - 1), j = 0, \dots, N_p - 1 \\ (A_{i-2,s}(k_i - 1) + B_{i-2,s}K)x_{i-2}^*(k_i + N_p - 1|k_i - 1), j = N_p. \end{cases} \tag{18}$$

3.2. ET-DMPC Controller Design

The traditional DMPC is a time-triggered control algorithm, i.e., it needs to solve the control optimization problem at each moment and transfer the information periodically to the unit trains connected to its topology, whereas the DMPC algorithm based on the ET mechanism solves the optimization problem and transfers the information at the triggering moment only, so it saves a large amount of communication resources and computational resources. As shown in Figure 3, the block diagram of the ET-DMPC algorithm designed in this paper, when the system satisfies the triggering conditions, the train state information will be passed to the controller, otherwise it will not be passed. The solid line in Figure 3 indicates that the information is transmitted regularly, while the dotted line indicates that the information is transmitted non-regularly.

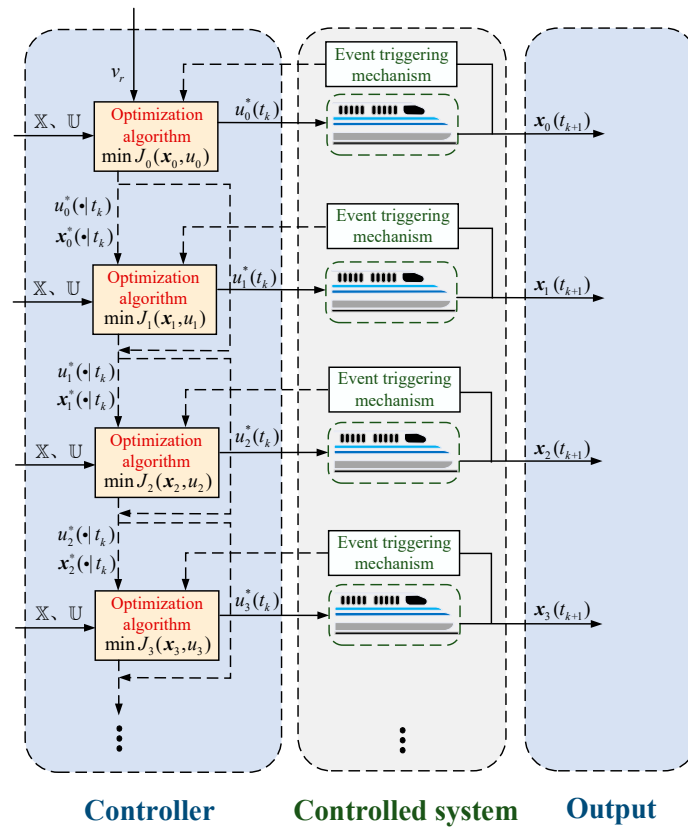


Figure 3. Block diagram of event-triggered distributed predictive control architecture.

The specific values of the state and control quantities to be transferred to the rear train are as follows, considering the two cases that the system satisfies the trigger condition and does not satisfy the trigger condition.

When the system satisfies the trigger condition at time k_i^d , the optimal control problem (12) is solved to obtain the optimal solution sequences $u_i^*(\cdot|k_i^d) = \{u_i^*(k_i^d + j|k_i^d) : j = 0, 1, \dots, N_p - 1\}$ and $x_i^*(\cdot|k_i^d) = \{x_i^*(k_i^d + j|k_i^d) : j = 0, 1, \dots, N_p\}$, and then, the feasible control quantities and the corresponding feasible state quantities at the next moment can be expressed as follows:

$$\bar{u}_i(k_i^d + j + 1|k_i^d + 1) = \begin{cases} u_i^*(k_i^d + j + 1|k_i^d), j = 0, \dots, N_p - 2 \\ \mathbf{K}\bar{x}_i(k_i^d + N_p|k_i^d + 1) + \mathbf{C}_i(k_i^d), j = N_p - 1. \end{cases} \quad (19)$$

$$\bar{x}_i(k_i^d + j + 1|k_i^d + 1) = \begin{cases} x_i^*(k_i^d + j + 1|k_i^d), j = 0, \dots, N_p - 1 \\ (\mathbf{A}_{i,s}(k_i^d) + \mathbf{B}_{i,s}\mathbf{K})\bar{x}_i(k_i^d + N_p|k_i^d + 1), j = N_p. \end{cases} \quad (20)$$

where \mathbf{K} is the state feedback gain matrix for train i .

When the system does not satisfy the trigger condition at moment k_i^d , then the optimal control problem is not solved at that moment, and then, the feasible control quantities at the next moment and the corresponding feasible state quantities can be expressed as follows:

$$\bar{u}_i(k_i^d + j + 1|k_i^d + 1) = \begin{cases} \bar{u}_i(k_i^d + j + 1|k_i^d), j = 0, \dots, N_p - 2 \\ \mathbf{K}\bar{x}_i(k_i^d + N_p|k_i^d + 1) + \mathbf{C}_i(k_i^d), j = N_p - 1. \end{cases} \quad (21)$$

$$\bar{x}_i(k_i^d + j + 1|k_i^d + 1) = \begin{cases} \bar{x}_i(k_i^d + j + 1|k_i^d), j = 0, \dots, N_p - 1 \\ (\mathbf{A}_{i,s}(k_i^d) + \mathbf{B}_{i,s}\mathbf{K})\bar{x}_i(k_i^d + N_p|k_i^d + 1), j = N_p. \end{cases} \quad (22)$$

Therefore, the feasible control sequence and the feasible state sequence of the system between the trigger moment k_i^d and the next trigger moment k_i^{d+1} , i.e., at time $k_i^d + h \in [k_i^d, k_i^{d+1}]$, can be expressed as follows:

$$\bar{u}_i(k_i^d + j | k_i^d + h) = \begin{cases} u_i^*(k_i^d + j | k_i^d), j = h, \dots, N_p - 1 \\ \mathbf{K}\bar{x}_i(k_i^d + j | k_i^d + h) + \mathbf{C}_i(k_i^d + h - 1), j = N_p, \dots, N_p - 1 + h. \end{cases} \quad (23)$$

$$\bar{x}_i(k_i^d + j | k_i^d + h) = \begin{cases} x_i^*(k_i^d + j | k_i^d), j = h, \dots, N_p \\ (\mathbf{A}_{i,s}(k_i^d + h - 1) + \mathbf{B}_{i,s}\mathbf{K})\bar{x}_i(k_i^d + j | k_i^d + h), j = N_p + 1, \dots, N_p + h. \end{cases} \quad (24)$$

where $h = k_i - k_i^d (1 \leq h \leq N_p - 1)$.

In summary, the VCTS control optimization problem based on the ET-DMPC algorithm is described as follows:

Problem 1.

$$\min_{u_i(\cdot | k_i^d)} J_i(x_i(\cdot | k_i^d), u_i(\cdot | k_i^d)) = W_i(x_i(\cdot | k_i^d), u_i(\cdot | k_i^d)) + M_i(x_i(\cdot | k_i^d), u_i(\cdot | k_i^d)) \quad (25)$$

$$s.t. x_i(k_i^d + j + 1 | k_i^d) = \mathbf{A}_{i,s}(k_i^d) x_i(k_i^d + j | k_i^d) + \mathbf{B}_{i,s} u_i(k_i^d + j | k_i^d) + \mathbf{C}_{i,s}(k_i^d) \quad (25a)$$

$$x_i(k_i^d + j | k_i^d) \in \mathbb{X}_i, j = 1, \dots, N_p - 1 \quad (25b)$$

$$u_i(k_i^d + j | k_i^d) \in \mathbb{U}_i, j = 0, \dots, N_p - 1 \quad (25c)$$

$$x_i(k_i^d + N_p | k_i^d) \in \mathbb{X}_{if} \quad (25d)$$

$$\|\bar{x}_i(k_i^d + j | k_i^d) - \hat{x}_i(k_i^d + j | k_i^d)\| \leq \bar{\zeta}_i(k_i^d), j = 1, \dots, N_p - 1 \quad (25e)$$

where $\bar{\zeta}_i(k_i)$ is the upper bound on the error of the feasible state quantity $\bar{x}_i(k_i + j | k_i)$ and the estimated state quantity $\hat{x}_i(k_i + j | k_i)$.

3.3. Event Trigger Condition

In order to ensure the stability requirement of the system, we will derive the event triggering condition of the system at time k_i^d in the following.

Consider a system triggered to solve a control optimization problem at two moments k_i^d and k_i^{d+1} , then $\bar{J}_i(k_i)$ is the cost function under the action of the feasible control sequence and the feasible state sequence at moment $k_i \in [k_i^d, k_i^{d+1}]$. If $k_i^d + h$ is between k_i^d and k_i^{d+1} , then $\Delta \bar{J}_i(k_i^d + h)$ is the difference between $\bar{J}_i(k_i^d + h)$ and $\bar{J}_i(k_i^d + h - 1)$.

Theorem 1. For the VCTS system (6), consider that the system satisfies the requirements of Assumption 1, and if its event triggering condition is designed as (26), it can be obtained that $\Delta \bar{J}_i(k_i^d + h) < 0$.

$$\Phi_{i1} + \Phi_{i2} > \sigma_i \Psi_i \quad (26)$$

In the formula,

$$\begin{aligned} \Psi_i &= \left\| x_i(k_i^d + h - 1 | k_i^d) \right\|_{\mathbf{Q}}^2 + \left\| u_i(k_i^d + h - 1 | k_i^d) \right\|_{\mathbf{R}}^2 \\ &+ \left\| x_i(k_i^d + h - 1 | k_i^d) - \hat{x}_{i-1}(k_i^d + h - 1 | k_i^d + h - 1) \right\|_{\mathbf{P}}^2 + \left\| x_i(k_i^d + h - 1 | k_i^d) - \hat{x}_{i-2}(k_i^d + h - 1 | k_i^d + h - 1) \right\|_{\mathbf{P}}^2 \end{aligned} \quad (27)$$

$$\Phi_{i1} = \sum_{j=0}^{N_p-2} \bar{\lambda}(\mathbf{P}) [2(\zeta_i(k_i^d + h + j | k_i^d + h) + \eta_{i-1}(k_i^d + h + j | k_i^d + h)) \cdot \zeta_{i-1}(k_i^d + h + j | k_i^d + h) + \zeta_{i-1}^2(k_i^d + h + j | k_i^d + h)] \quad (28)$$

$$\Phi_{i2} = \sum_{j=0}^{N_p-2} \bar{\lambda}(\mathbf{P}) [2(\xi_i(k_i^d + h + j|k_i^d + h) + \eta_{i-2}(k_i^d + h + j|k_i^d + h)) \cdot \xi_{i-2}(k_i^d + h + j|k_i^d + h) + \xi_{i-2}^2(k_i^d + h + j|k_i^d + h)] \quad (29)$$

$$\begin{aligned} \text{where, } \xi_i(k_i^d + h + j|k_i^d + h) &= \left\| \bar{\mathbf{x}}_i(k_i^d + h + j|k_i^d + h) - \hat{\mathbf{x}}_i(k_i^d + h + j|k_i^d + h) \right\|, \\ \eta_{i-1}(k_i^d + h + j|k_i^d + h) &= \left\| \hat{\mathbf{x}}_i(k_i^d + h + j|k_i^d + h) - \hat{\mathbf{x}}_{i-1}(k_i^d + h + j|k_i^d + h) \right\|, \\ \eta_{i-2}(k_i^d + h + j|k_i^d + h) &= \left\| \hat{\mathbf{x}}_i(k_i^d + h + j|k_i^d + h) - \hat{\mathbf{x}}_{i-2}(k_i^d + h + j|k_i^d + h) \right\|. \end{aligned}$$

Proof of Theorem 1. See Appendix A. \square

Remark 3. Due to $1 \leq h \leq N_p - 1$, consider forcing the ET-DMPC optimization problem to be solved if no event triggering condition occurs in the system in the prediction time domain N_p . Therefore, the event trigger condition can be described as follows:

$$\Phi_{i1} + \Phi_{i2} > \sigma_i \Psi_i \text{ or } k_i = k_i^d + N_p \quad (30)$$

Remark 4. For the event triggering condition (30), the smaller σ_i is, the easier the event triggering condition can be satisfied, but at the same time, it will increase the communication cost and computation cost. In particular, when $\sigma_i = 0$, ET-DMPC becomes DMPC, and the event triggering mechanism fails. As σ_i increases, the number of system triggers decreases, but at the same time, the algorithm control performance decreases. Therefore, it is necessary to choose an appropriate trigger parameter to achieve a balance between the system control performance and resource utilization.

The ET-DMPC algorithm proposed in this paper is described in Algorithm 1 as follows:

Algorithm 1 The ET-DMPC algorithm

Initialization: Set the train performance parameters, the reference speed curve $v_r(t)$, the speed limit curve $v_{\lim}(s(t))$, the fixed inter-company distance d_0 , the braking safety margin d_{safe} and the initial state $\mathbf{x}_i(0)$ of the train in each unit. Define the system parameters $N_p, \mathbf{K}, \mathbf{H}, \mathbf{Q}, \mathbf{P}, \mathbf{R}$; let $i = 0, k_i = 0, \hat{\mathbf{x}}_i(j|0) = 0 (j = 1, \dots, N_p - 1)$.

Step 1: Solve Problem 1 to obtain the optimal control sequence

$u_i^*(\cdot|0) = \{u_i^*(j|0) : j = 0, 1, \dots, N_p - 1\}$ at the moment $k_i = 0$, and then, obtain the optimal predicted state $\mathbf{x}_i^*(\cdot|0) = \{\mathbf{x}_i^*(j|0) : j = 0, 1, \dots, N_p\}$ at that moment, apply the control quantity $u_i^*(0|0)$ to the unit train, and transfer the optimal predicted state sequence to the topologically connected unit train.

Step 2: At the moment $k_i > 0$, judge whether the event trigger condition (30) is satisfied:

- (1) If satisfied, then $k_i^d = k_i$, the controller solves Problem 1 based on the actual state quantities at that moment and the predicted state sequences of the topologically connected trains, obtains the optimal control sequence $u_i^*(\cdot|k_i^d) = \{u_i^*(k_i^d + j|k_i^d) : j = 0, 1, \dots, N_p - 1\}$ at that moment and then obtains the optimal predicted state $\mathbf{x}_i^*(\cdot|k_i^d) = \{\mathbf{x}_i^*(k_i^d + j|k_i^d) : j = 0, 1, \dots, N_p\}$ at the corresponding moment, applies the control quantities $u_i^*(k_i^d|k_i^d)$ to the train, and passes the optimal predicted state sequences to the trains of its topologically connected units.
- (2) If not, problem 1 is not solved, the controller acts on the unit train according to the feasible control sequences and feasible state sequences obtained from (23) and (24) and does not pass the information to the topologically connected trains, and the controllers of the topologically connected unit trains also solve the control quantities of the unit train according to the feasible control sequences and feasible state sequences of the forward train obtained from (23) and (24).

Step 3: Let $k_i = k_i + 1$, return to step 2.

In order to describe the above algorithm steps more intuitively, the flowchart of the designed algorithm is shown in Figure 4.

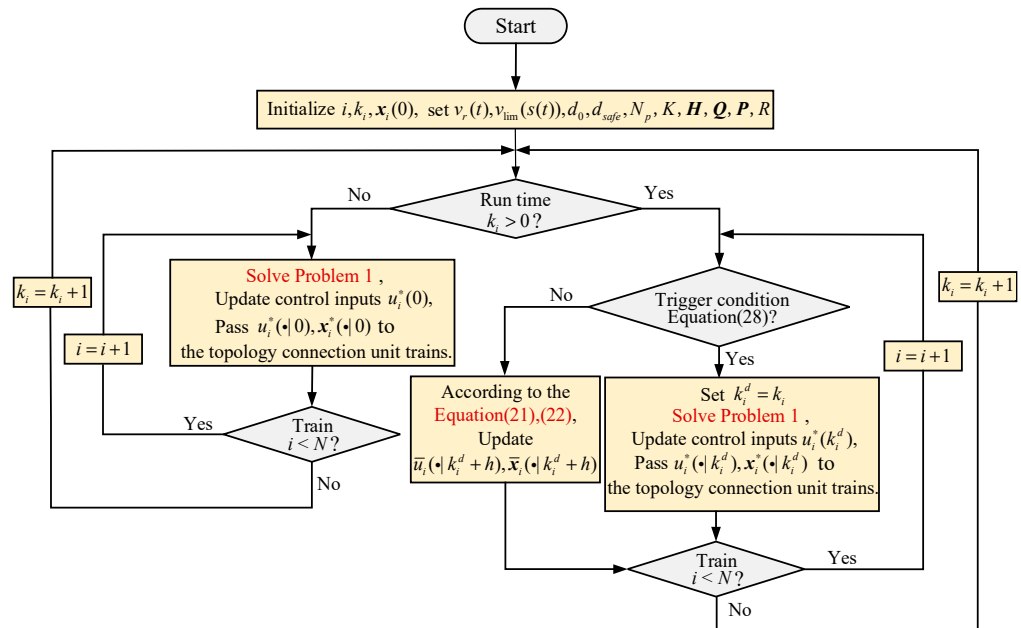


Figure 4. ET-DMPC algorithm flowchart.

3.4. Recursive Feasibility

In order to prove the algorithmic feasibility of ET-DMPC, a recursive feasibility analysis of the ET-DMPC algorithm is given in this section.

Theorem 2. Assuming that there is a feasible solution to the constrained optimization problem 1 at time $k = k_i^d$, then for any time $k > k_i^d$, there is a feasible solution to the constrained optimization problem.

Proof of Theorem 2. Assuming that the system triggers the solving of problem 1 at the moment k_i^d and solves the optimal control sequence $u_i^*(k_i^d + j|k_i^d) \in \mathbb{U}_i$ and the corresponding optimal state sequence $x_i^*(k_i^d + j|k_i^d) \in \mathbb{X}_i$, it is necessary to prove that at the moment $k > k_i^d$, without triggering the solving problem 1, the feasible control sequences and the feasible state sequences under the operation of (23) and (24) still satisfy the constraints (25b)–(25e), and then, the system is recursively feasible.

For time $k_i^d + 1$, the feasible control sequence $\bar{u}_i(k_i^d + j + 1|k_i^d + 1) = u_i^*(k_i^d + j + 1|k_i^d) \in \mathbb{U}_i$ ($j = 0, \dots, N_p - 2$) and the feasible state sequence $\bar{x}_i(k_i^d + j + 1|k_i^d + 1) = x_i^*(k_i^d + j + 1|k_i^d) \in \mathbb{X}_i$ ($j = 0, \dots, N_p - 1$) are constructed according to the $u_i^*(k_i^d + j|k_i^d)$ and $x_i^*(k_i^d + j|k_i^d)$ obtained at time k_i^d . It can be seen from Assumption 1 that when $j = N_p - 1$, $\bar{u}_i(k_i^d + N_p|k_i^d + 1) = \mathbf{K}x_i^*(k_i^d + N_p|k_i^d) + \mathbf{C}_i(k_i^d) \in \mathbb{U}_i$, and $j = N_p$, $\bar{x}_i(k_i^d + N_p + 1|k_i^d + 1) = (\mathbf{A}_{i,s}(k_i^d) + \mathbf{B}_{i,s}\mathbf{K})x_i^*(k_i^d + N_p|k_i^d) \in \mathbb{X}_{if} \subset \mathbb{X}_i$;

For time $k_i^d + h \in [k_i^d + 1, k_i^{d+1}]$, according to the $\bar{u}_i(k_i^d + h - 1 + j|k_i^d + h - 1)$ and $\bar{x}_i(k_i^d + h - 1 + j|k_i^d + h - 1)$ constructed at the previous time, the feasible control sequence $\bar{u}_i(k_i^d + h + j|k_i^d + h) = \bar{u}_i(k_i^d + h + j|k_i^d + h - 1) \in \mathbb{U}_i$ ($j = 0, \dots, N_p - 2$) and the feasible state sequence $\bar{x}_i(k_i^d + h + j|k_i^d + h) = \bar{x}_i(k_i^d + h + j|k_i^d + h - 1) \in \mathbb{X}_i$ ($j = 0, \dots, N_p - 1$) of the time are constructed. Similarly, when $j = N_p - 1$, $\bar{u}_i(k_i^d + h + N_p - 1|k_i^d + h) = \mathbf{K}\bar{x}_i(k_i^d + h + N_p - 1|k_i^d + h) + \mathbf{C}_i(k_i^d + h - 1) \in \mathbb{U}_i$, and $j = N_p$, $\bar{x}_i(k_i^d + h + N_p|k_i^d + h) = (\mathbf{A}_{i,s}(k_i^d + h - 1) + \mathbf{B}_{i,s}\mathbf{K})\bar{x}_i(k_i^d + h + N_p - 1|k_i^d + h) \in \mathbb{X}_{if} \subset \mathbb{X}_i$.

In summary, at $k_i^d + h \in [k_i^d, k_i^{d+1}]$, the control constraints, state constraints, and terminal state constraints (25b)–(25d) all meet the requirements.

For time $k_i^d + 1$, $\bar{x}_i(k_i^d + 1 + j|k_i^d + 1) = \hat{x}_i(k_i^d + 1 + j|k_i^d + 1) = x_i^*(k_i^d + j|k_i^d)$ ($j = 0, \dots, N_p - 1$), when $j = N_p$, $\bar{x}_i(k_i^d + 1 + N_p|k_i^d + 1) = \hat{x}_i(k_i^d + 1 + N_p|k_i^d + 1) = (A_{i,s}(k_i^d) + B_{i,s}K)x_i^*(k_i^d + N_p|k_i^d)$, therefore, $\|\bar{x}_i(k_i^d + 1 + j|k_i^d + 1) - \hat{x}_i(k_i^d + 1 + j|k_i^d + 1)\| = 0 \leq \bar{\xi}_i(k_i^d + 1)$;

For time $k_i^d + h \in [k_i^d + 1, k_i^{d+1}]$, $\bar{x}_i(k_i^d + h + j|k_i^d + h) = \hat{x}_i(k_i^d + h + j|k_i^d + h) = \bar{x}_i(k_i^d + h - 1 + j|k_i^d + h - 1)$ ($j = 0, \dots, N_p - 1$), when $j = N_p$, $\bar{x}_i(k_i^d + h + N_p|k_i^d + h) = \hat{x}_i(k_i^d + h + N_p|k_i^d + h) = (A_{i,s}(k_i^d + h - 1) + B_{i,s}K)\bar{x}_i(k_i^d + h + N_p - 1|k_i^d + h)$, therefore, $\|\bar{x}_i(k_i^d + h + j|k_i^d + h) - \hat{x}_i(k_i^d + h + j|k_i^d + h)\| = 0 \leq \bar{\xi}_i(k_i^d + h)$.

In summary, at $k_i^d + h \in [k_i^d, k_i^{d+1}]$, the error constraint (25e) between the feasible state quantity and the estimated state quantity meets the requirements. \square

3.5. Closed-Loop Stability

In order to ensure the closed-loop stability of the system, the sufficient condition to ensure the input-state stability (ISS) of the system is given in this section.

Define 1. Given a function $\chi(k)$, the domain is $k \in [0, a)$, and a is a positive real number. If $\chi(0) = 0$ and $\chi(k)$ satisfy continuous and strictly increasing, it is called a K -class function.

Define 2. Given a function $\chi(k)$, the domain is $k \in [0, \infty)$. If $\chi(k)$ satisfies the condition of Define 1, when $k \rightarrow \infty$, $\chi(k) = \infty$, then it is called a K_∞ function.

Define 3. If the Lyapunov function $J(k)$ of the system satisfies the following two conditions, then $J(k)$ is an ISS-Lyapunov function:

- 1) $\chi_1(x(k)) \leq J(k) \leq \chi_2(x(k))$, where $x(k) \in \mathbb{R}^n$, χ_1 and χ_2 are K_∞ functions;
- 2) $J(k + 1) - J(k) \leq -\chi_3(x(k)) + \omega(\bar{\xi}(k))$, where $x(k) \in \mathbb{R}^n$ and χ_3 are K_∞ functions and ω are a K functions.

Lemma 1. If there is an ISS-Lyapunov function, the system is ISS.

Theorem 3. For the VCTS system (6), if its event-triggered condition satisfies the following, then the system is ISS:

$$\bar{\xi}_i(k_i^d) \leq \bar{\eta}_i(k_i^d) \tag{31}$$

$$\text{where } \bar{\eta}_i(k_i^d) = \max_{\substack{i = i - 1 \\ i = i - 2}} \left(\max_{1 \leq j \leq N_p - 1} (\eta_i(k_i^d + j|k_i^d)) \right).$$

Proof of Theorem 3. See Appendix B. \square

4. Simulation Experiment and Analysis

In order to verify the effectiveness of the proposed method, a semi-physical simulation platform equipped in the laboratory for high-speed train tracking operation is used for simulation experiments. The VCTS consisting of four CRH380A unit trains is used as the control object. The simulation of the whole process of running trains out, into the station, as shown in Figure 5, is the tracking of the leader of the train operating speed curve and displacement curve, which includes the train acceleration, idling, braking, and three kinds of operating conditions, and in different sections of the road, the limit of the speed of the value is different. The sampling interval of the system is 1s, and the number of collected samples is 3000. The specific parameters of the simulation system are shown in Table 1.

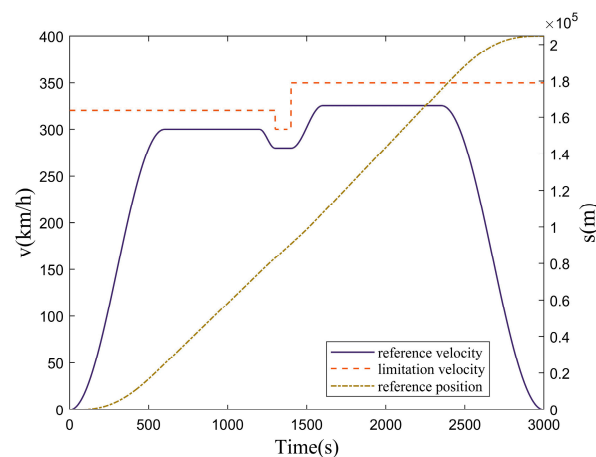


Figure 5. Leader train tracking reference curve.

Table 1. System parameter.

Parameters	Parameters Values	Unit
Unit train mass m_i	480, 485, 482, 484	t
Drag coefficient c_0	0.7550	N/kg
Drag coefficient c_1	0.00636	N/(km/h kg)
Drag coefficient c_2	0.000115	N/(km ² /h ² kg)
Fixed Follower Distance d_0	100	m
Brake safety margin d_{safe}	50	m
maximum acceleration U_{max}	1	m/s ²
maximum deceleration U_{min}	-1	m/s ²

The experiments in this paper are divided into two groups: The first group of experiments uses the ET-DMPC method proposed in this paper when the triggering parameter $\sigma_i = 0$ in the train operating range of the simulation experiments on four unit trains, to assess the performance and efficiency of the algorithm and compare it with the traditional CMPC, in order to validate the effectiveness of this paper's algorithm for the coordinated tracking control of the VCTS. In the second group of experiments, the ET-DMPC method with different triggering parameters is used to simulate the VCTS, the train tracking efficiency, and resource consumption under each triggering parameter, which are compared and analyzed to verify the effectiveness of this paper's algorithm in saving the communication and computation resources of the system.

4.1. Experiment 1: Comparative Analysis of Algorithm Tracking Performance

In order to verify the effectiveness of this paper's method on the cooperative tracking control of virtual formation trains, in this experiment, we use the traditional CMPC method and the proposed ET-DMPC method (with the trigger parameter $\sigma_i = 0$) for the formation tracking control of four unit trains, respectively. The initial error states of the four unit trains are all set to zero, i.e., the VCTS is in a stable stopping state. The parameter settings of the method controller and CMPC method controller in this paper are shown in Tables 2 and 3.

Table 2. ET-DMPC controller parameter.

Parameters	Parameters Values
Predictive time domain N_p	10
Weighting matrix Q	[0.8,0.8,0.4]
Weighting matrix P	[0.6,0.6,0.3]
Weighting matrix R	0.3
Weighting matrix H	[0.5,0.5,0.5]

Table 3. CMPC controller parameter.

Parameters	Parameters Values
Predictive time domain N_p	10
Weighting matrix Q	[0.8,0.8,0.8,0.8,0.4,0.4,0.4]
Weighting matrix R	[0.3,0.3,0.3]
Weighting matrix H	[0.5,0.5,0.5,0.5,0.5,0.5,0.5]

The state space equations under the CMPC method are set as follows:

$$\dot{x}(t) = A_c(t)x(t) + B_c u(t) + C_c(t) \tag{32}$$

where the control input matrix $u(t) = [u_0(t), u_1(t), u_2(t), u_3(t)]^T$; the output state matrix $x(t) = [e_{0,r}^v(t), e_{1,0}^v(t), e_{2,1}^v(t), e_{3,2}^v(t), e_{1,0}^s(t), e_{2,1}^s(t), e_{3,2}^s(t)]^T$; and each parameter matrix is expressed as:

$$A_c(t) = \begin{bmatrix} h/m_0 & 0 & 0 & 0 & 0 & 0 & 0 \\ 0 & 2h/(m_0 + m_1) & 0 & 0 & 0 & 0 & 0 \\ 0 & 0 & 2h/(m_1 + m_2) & 0 & 0 & 0 & 0 \\ 0 & 0 & 0 & 2h/(m_2 + m_3) & 0 & 0 & 0 \\ 0 & 1 & 0 & 0 & 0 & 0 & 0 \\ 0 & 0 & 1 & 0 & 0 & 0 & 0 \\ 0 & 0 & 0 & 1 & 0 & 0 & 0 \end{bmatrix}, B_c = \begin{bmatrix} -1 & 0 & 0 & 0 \\ 1 & -1 & 0 & 0 \\ 0 & 1 & -1 & 0 \\ 0 & 0 & 1 & -1 \\ 0 & 0 & 0 & 0 \\ 0 & 0 & 0 & 0 \\ 0 & 0 & 0 & 0 \end{bmatrix}$$

$$C_c(t) = \left[u_r(t) \quad 0 \quad 0 \quad 0 \quad -u_0(t) - \frac{h}{m_0}v_0(t) - \frac{c}{m_0} \quad -u_1(t) - \frac{h}{m_1}v_1(t) - \frac{c}{m_1} \quad -u_2(t) - \frac{h}{m_2}v_2(t) - \frac{c}{m_2} \right]^T$$

Figure 6 shows the speed error curves under the two control methods, and Figure 7 shows the distance error curves under the two control methods. In Figures 6a and 7a, the range of speed error between each unit train under the CMPC method are $[-1.0547, 1.0795]$, $[-0.9197, 0.9326]$, and $[-0.8059, 0.8060]$, respectively, and the range of distance error are $[-2.7748, 2.7574]$, $[-1.4861, 1.4751]$, and $[-0.1311, 0.1351]$, respectively. Whereas in Figures 6b and 7b, the range of the speed error between each unit train under the method of this paper are $[-0.7878, 0.7882]$, $[-0.7882, 0.7887]$, and $[-0.7887, 0.7893]$, respectively, and the range of distance error are $[-0.0625, 0.0624]$, $[-0.0625, 0.0700, 0.0699]$, and $[-0.0625, 0.0923, 0.0922]$, respectively. It can be seen that the speed error and distance error of each unit train under the method of this paper have a smaller range of fluctuation than that under the CMPC method. As shown in Figure 8, the acceleration curves of each unit train under the two control methods are shown; under the method of this paper, the controlled acceleration of each unit train is guaranteed to be between $[-0.2189, 0.2190]$, which satisfies the comfort criterion of train operation.

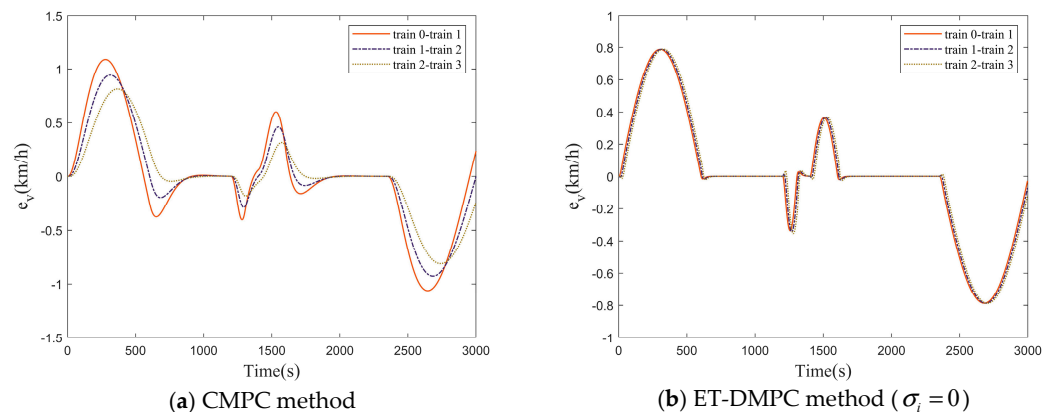


Figure 6. Velocity tracking error curve under two control methods.

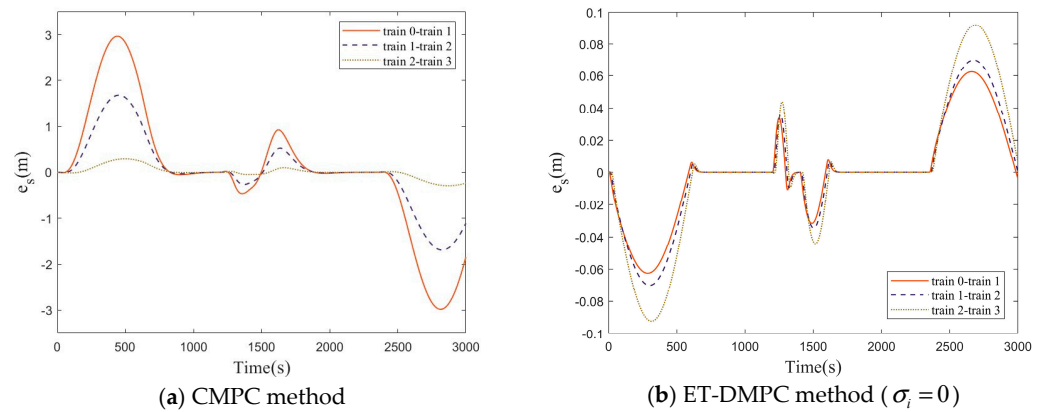


Figure 7. Distance tracking error curve under two control methods.

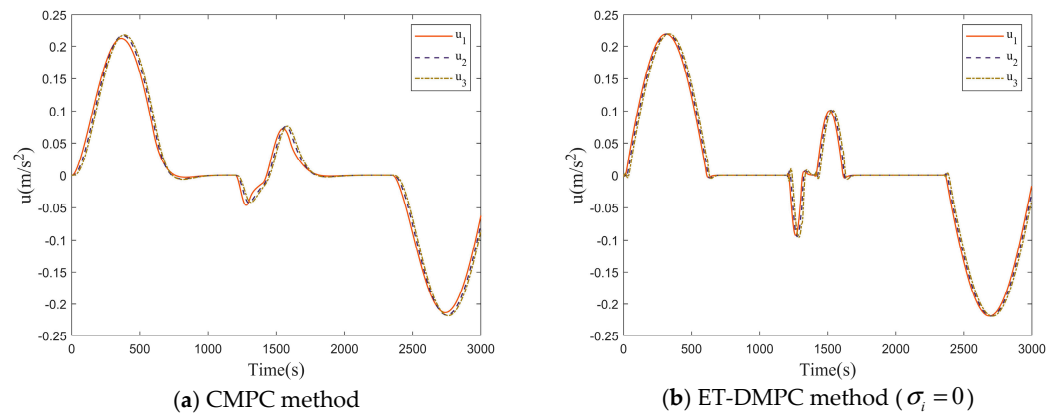


Figure 8. Control output curve under two control methods.

In order to analyze the control performance of each control algorithm more intuitively, we consider calculating the root-mean-square error ($MSEe_v$) of velocity and the root-mean-square error ($MSEe_s$) of distance of each controller according to (33) and (34) for the performance evaluation.

$$MSEe_v = \frac{1}{nT} \sum_{i=1}^n \sum_{t=1}^T |e_v(t)|^2 \tag{33}$$

$$MSEe_s = \frac{1}{nT} \sum_{i=1}^n \sum_{t=1}^T |e_s(t)|^2 \tag{34}$$

The performance index values of the two control methods are shown in Table 4, the smaller the MSE index value, the more accurate the tracking effect of the system and the better the control algorithm. It can be seen that the $MSEe_v$ and $MSEe_s$ of this paper’s method are smaller than that of the CMPC method. Therefore, the validity of this method for the cooperative tracking control of VCTS is verified.

Table 4. Comparison of algorithm performance indicators.

Methods	$MSEe_v$	$MSEe_s$
CMPC	0.0139	0.6828
ET-DMPC($\sigma_i = 0$)	0.0105	0.0013

Remark 5. ET-DMPC method with triggering parameter $\sigma_i = 0$, the event triggering mechanism is invalidated, i.e., the ET-DMPC method is downgraded to a DMPC method.

4.2. Experiment 2: Performance Analysis under Different Trigger Parameters

In Experiment 1, we use the ET-DMPC with the trigger parameter $\sigma_i = 0$ to verify the effectiveness of the VCTS cooperative tracking control method, each unit train controller needs to calculate the optimal control quantity and transfer the information at each sampling moment, but in the actual operation, the computational and communication resources are usually very limited, which is not conducive to the actual operation of VCTS. Therefore, in order to verify the effectiveness of the ET-DMPC method proposed in this paper, in saving the communication and computational resources of the system, we use the ET-DMPC method with different triggering parameters for the formation tracking control of four unit trains in this experiment. The initial state of each unit train is the same as that of Experiment 1, the control parameters are set as shown in Table 2, and the calculation time, number of triggers, and various control performance indexes are compared and analyzed under the three cases of trigger parameters $\sigma_i = 0, \sigma_i = 0.2$ and $\sigma_i = 0.8$.

In order to ensure the accuracy of the experiment, the simulation calculation time under each trigger parameter is taken as the average value of 10 texts. As shown in Table 5, the larger the trigger parameter is, the shorter the simulation time is. It can be seen that after the implementation of the event triggering mechanism, the simulation time of the system is greatly reduced. Figure 9 shows the trigger schedule when $\sigma_i = 0.2, \sigma_i = 0.8$. Among them, the trigger state of 1 indicates that the system is triggered by (24), and the trigger state of 2 indicates that the system is triggered by $k_i = k_i^d + N_p$. The specific trigger times are shown in Table 6, and it can be seen that the higher the trigger parameter is set, the fewer the number of controller triggers, and the lighter the burden of the system communication and computation. Therefore, it is verified that the method proposed in this paper is effective in saving the communication and computation resources of the system.

Table 5. Simulation operation time for each trigger parameter.

Trigger Parameter	Computation Time (Unit: s)					Average Value
$\sigma_i = 0$	Text1	Text2	Text3	Text4	Text5	43.9185
	46.9122	45.5438	42.4341	45.4474	45.4474	
	Text6	Text7	Text8	Text9	Text10	
44.4474	42.4055	42.3939	40.9397	43.2134		
$\sigma_i = 0.2$	Text1	Text2	Text3	Text4	Text5	30.5881
	32.3413	31.5088	30.0283	29.8224	30.2487	
	Text6	Text7	Text8	Text9	Text10	
30.6158	31.2560	29.5115	29.7634	30.7851		
$\sigma_i = 0.8$	Text1	Text2	Text3	Text4	Text5	23.2860
	23.8976	24.6295	22.0668	22.5758	24.1623	
	Text6	Text7	Text8	Text9	Text10	
24.3212	21.0563	25.0542	23.0792	22.0169		

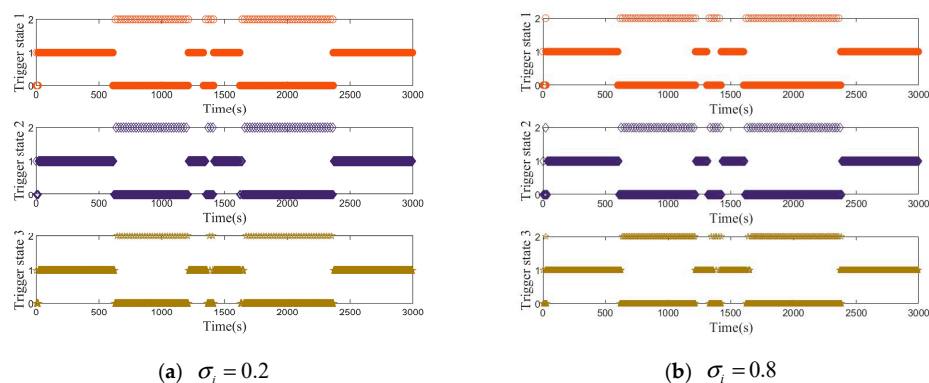


Figure 9. Trigger schedule.

Table 6. Different trigger parameter results.

	Train 1		Train 2		Train 3	
	Number of Triggers	Percentages	Number of Triggers	Percentages	Number of Triggers	Percentages
$\sigma_i = 0$	3000	100	3000	100	3000	100
$\sigma_i = 0.2$	1627	54.23	1652	55.07	1681	56.03
$\sigma_i = 0.8$	1538	51.27	1537	51.23	1567	52.23

However, as the trigger parameter increases, the control performance of the system decreases. Figures 10–12 show the speed tracking error curve, the distance error curve, and the control acceleration curve of each unit train under different triggering parameters, respectively. From these experimental simulation curves, we can see that as the trigger parameter increases, the curve fluctuation is larger, that is, the control performance is worse. Similarly, in order to analyze the control performance under each trigger parameter more intuitively, the relative error (RE) index of each control curve under different trigger parameters is calculated according to (35)–(37).

$$REe_v^{\sigma_i} = \frac{1}{T} \sum_{t=1}^T |e_v^{\sigma_i}(t) - e_v^{\sigma_i=0}(t)| \tag{35}$$

$$REe_s^{\sigma_i} = \frac{1}{T} \sum_{t=1}^T |e_s^{\sigma_i}(t) - e_s^{\sigma_i=0}(t)| \tag{36}$$

$$REu^{\sigma_i} = \frac{1}{T} \sum_{t=1}^T |u^{\sigma_i}(t) - u^{\sigma_i=0}(t)| \tag{37}$$

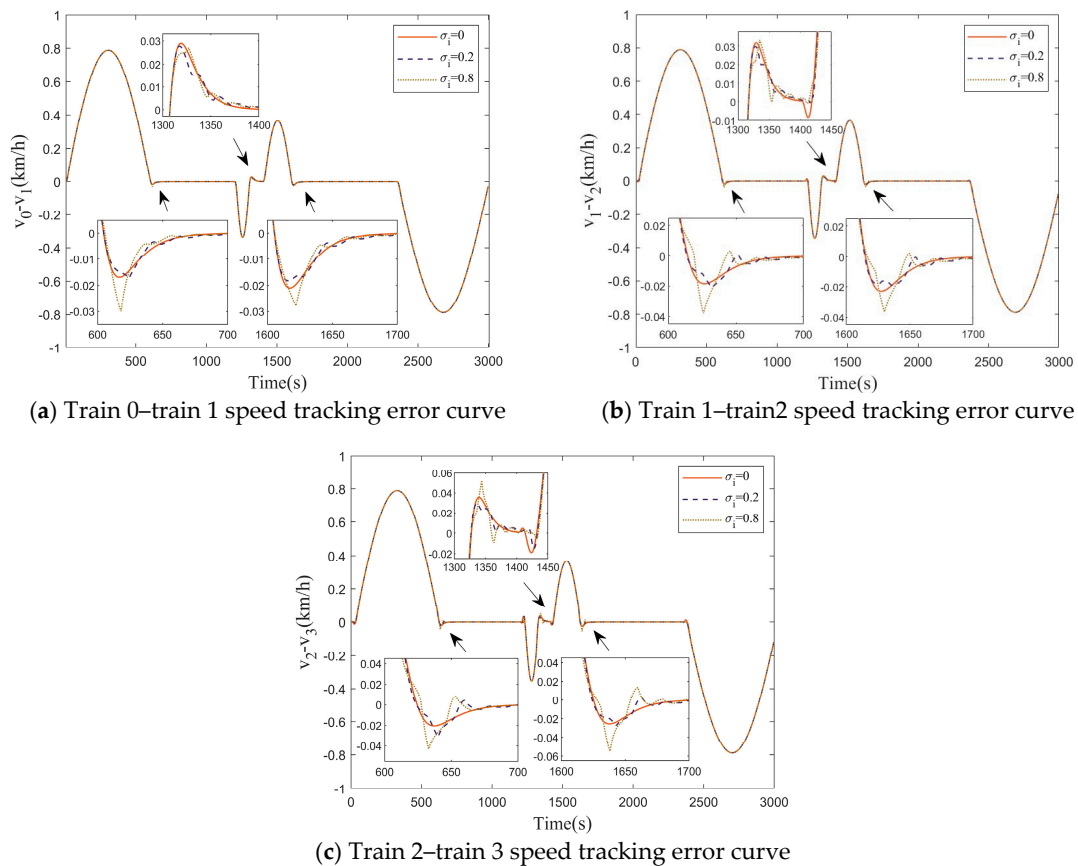


Figure 10. Velocity tracking error curves with different trigger parameters.

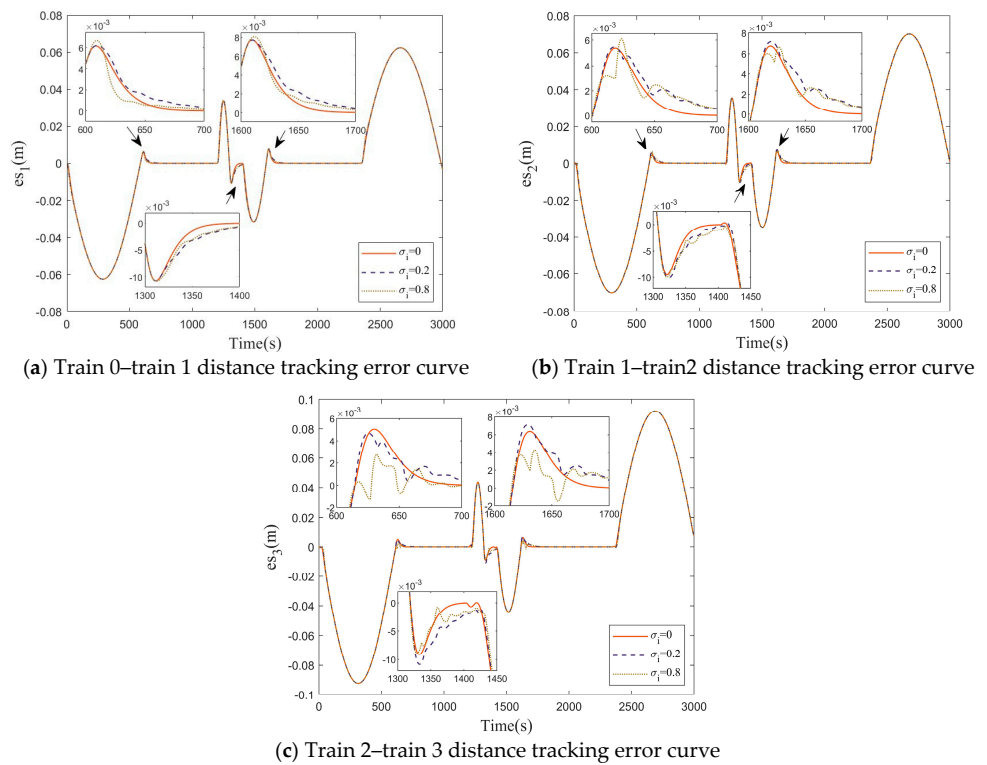


Figure 11. Distance tracking error curves with different trigger parameters.

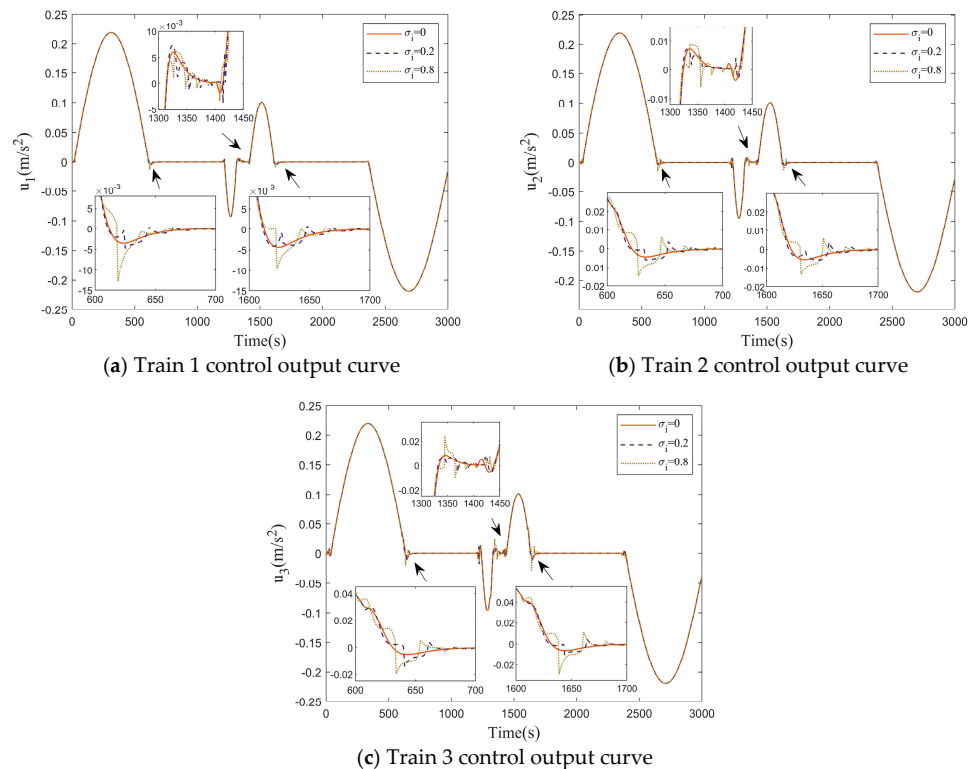


Figure 12. Control output curves with different trigger parameters.

The relative error index value under each trigger parameter is shown in Table 7, which shows that the larger the trigger parameter is, the larger the relative error value is. Therefore, as mentioned in Remark 3, a suitable event trigger parameter σ_i should

be selected in the actual control design to achieve a balance between the system control performance and resource utilization.

Table 7. Relative error.

		$\sigma_i=0$	$\sigma_i=0.2$	$\sigma_i=0.8$
Train 1	ev_1 relative error	0	5.3004×10^{-5}	1.0698×10^{-4}
	es_1 relative error	0	1.1469×10^{-4}	1.7109×10^{-4}
	u_1 relative error	0	1.0878×10^{-4}	2.0945×10^{-4}
Train 2	ev_2 relative error	0	8.9119×10^{-5}	2.1005×10^{-4}
	es_2 relative error	0	1.3411×10^{-4}	1.8198×10^{-4}
	u_2 relative error	0	1.6392×10^{-4}	3.8354×10^{-4}
Train 3	ev_3 relative error	0	1.5140×10^{-4}	3.4075×10^{-4}
	es_3 relative error	0	2.1348×10^{-4}	2.9483×10^{-4}
	u_3 relative error	0	3.1509×10^{-4}	6.6318×10^{-4}

Remark 6. *This experiment specifies the saving of communication and computation resources as the comparison of computation time and the number of triggers, in the case of fixed communication and computation resources, the higher the number of triggers, the more the communication and computation resources are occupied, the easier the communication network is blocked and the longer the computation time is. Therefore, in order to save computational and communication resources, the system should be triggered as few times as possible. But at the same time, it is necessary to ensure a certain degree of the control performance.*

5. Conclusions

In this paper, an ET-DMPC method for VCTS operation control is proposed. Firstly, an improved DMPC algorithm is proposed for the VCTS cooperative tracking control problem, which describes the VCTS control problem under the dual-leader topology as a set of optimal control problems with multiple constraints and considers the introduction of the state information of the neighboring systems into the performance index function to make the formation more stable. Secondly, due to the limitation of communication resources and computational resources during the actual train operation, the ET mechanism is further introduced, and the ET conditions are designed according to the state information of the neighboring system and its own system, and an ET-DMPC method is proposed to reduce the impact of the resource limitation. Finally, a semi-physical simulation platform equipped in the laboratory is used to simulate the whole process of the train moving out-into the station. The simulation results show the following:

- (1) The tracking error of this paper's control method is smaller than that of the traditional CMPC method. Under this paper's control method, the maximum speed error of VCTS tracking is $[-0.7887, 0.7893]$, the maximum distance error is $[-0.0923, 0.0922]$, and the control acceleration is guaranteed to be within $[-0.2189, 0.2190]$, which meets the comfort standard of train operation. This validates the effectiveness of this paper's method for the cooperative tracking control of VCTS.
- (2) After the introduction of the ET mechanism, the simulation running time of the system is shortened, and as the trigger parameter is larger, the number of system triggers is less, which reduces the burden of system communication and computation, and verifies the effectiveness of this paper's method in saving the communication and computation resources.

Based on the research in this paper, the authors will further carry out the following research:

- (1) Consider adding a sliding time window and designing a dynamic event triggering condition [27], so that the system can adaptively set the triggering parameter to further improve the impact of the ET mechanism on the system control performance, and

- consider applying this method to the maglev train formation control system and other intelligent formation control systems, e.g., UAVs formation, vehicle formation, etc.
- (2) The control method in this paper is a model-based control method, but in the actual VCTS operation process, due to the complexity and variability of the operating environment, there will be uncertainty factors, resulting in inaccuracy of the system model parameters, so subsequent consideration will be given to model-based predictive control combined with a data-driven control strategy [28–30], or to design a self-adaptive model parameters of the control method [31].
 - (3) For VCTS in the presence of disturbances, designing controllers with strong robustness and low computational effort will also be the focus of subsequent research [32,33].

Author Contributions: Conceptualization, Z.L. and L.Z. (Lingyu Zhong); methodology, Z.L. and L.Z. (Lingyu Zhong); software, L.Z. (Lingyu Zhong); validation, H.Y., Z.L. and L.Z. (Liang Zhou); formal analysis, Z.L.; investigation, Z.L.; resources, H.Y.; writing—original draft preparation, L.Z. (Lingyu Zhong); writing—review and editing, Z.L., L.Z. (Lingyu Zhong) and L.Z. (Liang Zhou); funding acquisition, Z.L. and H.Y.; All authors have read and agreed to the published version of the manuscript.

Funding: This research was funded by the National Natural Science Foundation of China (61991404, 52162048, U2034211), Training Program for Academic and Technical Leaders of Major Disciplines of Jiangxi Province (20213BCJ22002), and Natural Science Foundation Project of Liaoning Province (2022-KF-21-03).

Data Availability Statement: Data are contained within the article.

Conflicts of Interest: The authors declare no conflict of interest.

Appendix A

According to (25), we can obtain

$$\begin{aligned}
 \Delta \bar{J}_i(k_i^d + h) &= \bar{J}_i(k_i^d + h) - \bar{J}_i(k_i^d + h - 1) \\
 &= \sum_{j=0}^{N_p-1} \left(\left\| \bar{x}_i(k_i^d + h + j | k_i^d + h) \right\|_{\mathcal{Q}}^2 + \left\| \bar{u}_i(k_i^d + h + j | k_i^d + h) \right\|_{\mathcal{R}}^2 \right) - \sum_{j=0}^{N_p-1} \left(\left\| \bar{x}_i(k_i^d + h - 1 + j | k_i^d + h - 1) \right\|_{\mathcal{Q}}^2 + \left\| \bar{u}_i(k_i^d + h - 1 + j | k_i^d + h - 1) \right\|_{\mathcal{R}}^2 \right) \\
 &+ \left\| \bar{x}_i(k_i^d + h + N_p | k_i^d + h) \right\|_{\mathcal{H}}^2 - \left\| \bar{x}_i(k_i^d + h - 1 + N_p | k_i^d + h - 1) \right\|_{\mathcal{H}}^2 \\
 &+ \sum_{j=0}^{N_p-1} \left(\left\| \bar{x}_i(k_i^d + h + j | k_i^d + h) - \hat{x}_{i-1}(k_i^d + h + j | k_i^d + h) \right\|_{\mathcal{P}}^2 \right) - \sum_{j=0}^{N_p-1} \left(\left\| \bar{x}_i(k_i^d + h - 1 + j | k_i^d + h - 1) - \hat{x}_{i-1}(k_i^d + h - 1 + j | k_i^d + h - 1) \right\|_{\mathcal{P}}^2 \right) \\
 &+ \sum_{j=0}^{N_p-1} \left(\left\| \bar{x}_i(k_i^d + h + j | k_i^d + h) - \hat{x}_{i-2}(k_i^d + h + j | k_i^d + h) \right\|_{\mathcal{P}}^2 \right) - \sum_{j=0}^{N_p-1} \left(\left\| \bar{x}_i(k_i^d + h - 1 + j | k_i^d + h - 1) - \hat{x}_{i-2}(k_i^d + h - 1 + j | k_i^d + h - 1) \right\|_{\mathcal{P}}^2 \right) \\
 &+ \left\| \bar{x}_i(k_i^d + h + N_p | k_i^d + h) - \hat{x}_{i-1}(k_i^d + h + N_p | k_i^d + h) \right\|_{\mathcal{H}}^2 - \left\| \bar{x}_i(k_i^d + h - 1 + N_p | k_i^d + h - 1) - \hat{x}_{i-1}(k_i^d + h - 1 + N_p | k_i^d + h - 1) \right\|_{\mathcal{H}}^2 \\
 &+ \left\| \bar{x}_i(k_i^d + h + N_p | k_i^d + h) - \hat{x}_{i-2}(k_i^d + h + N_p | k_i^d + h) \right\|_{\mathcal{H}}^2 - \left\| \bar{x}_i(k_i^d + h - 1 + N_p | k_i^d + h - 1) - \hat{x}_{i-2}(k_i^d + h - 1 + N_p | k_i^d + h - 1) \right\|_{\mathcal{H}}^2
 \end{aligned} \tag{A1}$$

Collating (A1), we can obtain

$$\Delta \bar{J}_i(k_i^d + h) = \Theta_{i1} + \Theta_{i2} + \Theta_{i3} - \Psi_i \tag{A2}$$

where

$$\begin{aligned}
 \Theta_{i1} &= \|\bar{x}_i(k_i^d + h - 1 + N_p | k_i^d + h)\|_Q^2 + \|\bar{u}_i(k_i^d + h - 1 + N_p | k_i^d + h)\|_R^2 \\
 &+ \|\bar{x}_i(k_i^d + h - 1 + N_p | k_i^d + h) - \hat{x}_{i-1}(k_i^d + h - 1 + N_p | k_i^d + h)\|_P^2 + \|\bar{x}_i(k_i^d + h - 1 + N_p | k_i^d + h) - \hat{x}_{i-2}(k_i^d + h - 1 + N_p | k_i^d + h)\|_P^2 \\
 &+ \|\bar{x}_i(k_i^d + h + N_p | k_i^d + h)\|_H^2 - \|\bar{x}_i(k_i^d + h - 1 + N_p | k_i^d + h - 1)\|_H^2 \\
 &+ \|\bar{x}_i(k_i^d + h + N_p | k_i^d + h) - \hat{x}_{i-1}(k_i^d + h + N_p | k_i^d + h)\|_H^2 - \|\bar{x}_i(k_i^d + h - 1 + N_p | k_i^d + h - 1) - \hat{x}_{i-1}(k_i^d + h - 1 + N_p | k_i^d + h - 1)\|_H^2 \\
 &+ \|\bar{x}_i(k_i^d + h + N_p | k_i^d + h) - \hat{x}_{i-2}(k_i^d + h + N_p | k_i^d + h)\|_H^2 - \|\bar{x}_i(k_i^d + h - 1 + N_p | k_i^d + h - 1) - \hat{x}_{i-2}(k_i^d + h - 1 + N_p | k_i^d + h - 1)\|_H^2 \tag{A3} \\
 &\leq \left\| \left((A_{i,s} + B_{i,s}K)^T H(A_{i,s} + B_{i,s}K) + Q - H + RK^T K \right) \bar{x}_i(k_i^d + h - 1 + N_p | k_i^d + h) \right\|^2 \\
 &+ \left\| \left((A_{i,s} + B_{i,s}K)^T H(A_{i,s} + B_{i,s}K) + P - H \right) \bar{x}_i(k_i^d + h - 1 + N_p | k_i^d + h) - \hat{x}_{i-1}(k_i^d + h - 1 + N_p | k_i^d + h) \right\|^2 \\
 &+ \left\| \left((A_{i,s} + B_{i,s}K)^T H(A_{i,s} + B_{i,s}K) + P - H \right) \bar{x}_i(k_i^d + h - 1 + N_p | k_i^d + h) - \hat{x}_{i-2}(k_i^d + h - 1 + N_p | k_i^d + h) \right\|^2 \\
 &\leq 0
 \end{aligned}$$

$$\begin{aligned}
 \Theta_{i2} &= \sum_{j=0}^{N_p-2} \left(\|\bar{x}_i(k_i^d + h + j | k_i^d + h) - \hat{x}_{i-1}(k_i^d + h + j | k_i^d + h)\|_P^2 - \|\bar{x}_i(k_i^d + h + j | k_i^d + h - 1) - \hat{x}_{i-1}(k_i^d + h + j | k_i^d + h - 1)\|_P^2 \right) \\
 &\leq \sum_{j=0}^{N_p-2} \bar{\lambda}(P) [2 \|\bar{x}_i(k_i^d + h + j | k_i^d + h) - \hat{x}_i(k_i^d + h + j | k_i^d + h) + \hat{x}_i(k_i^d + h + j | k_i^d + h) - \hat{x}_{i-1}(k_i^d + h + j | k_i^d + h)\| \\
 &\quad \times \|\bar{x}_{i-1}(k_i^d + h + j | k_i^d + h) - \hat{x}_{i-1}(k_i^d + h + j | k_i^d + h)\| + \|\bar{x}_{i-1}(k_i^d + h + j | k_i^d + h) - \hat{x}_{i-1}(k_i^d + h + j | k_i^d + h)\|^2] \tag{A4} \\
 &\leq \sum_{j=0}^{N_p-2} \bar{\lambda}(P) [2(\zeta_i(k_i^d + h + j | k_i^d + h) + \eta_{i-1}(k_i^d + h + j | k_i^d + h)) \cdot \zeta_{i-1}(k_i^d + h + j | k_i^d + h) + \zeta_{i-1}^2(k_i^d + h + j | k_i^d + h)] \\
 &= \Phi_{i1}
 \end{aligned}$$

$$\begin{aligned}
 \Theta_{i3} &= \sum_{j=0}^{N_p-2} \left(\|\bar{x}_i(k_i^d + h + j | k_i^d + h) - \hat{x}_{i-2}(k_i^d + h + j | k_i^d + h)\|_P^2 - \|\bar{x}_i(k_i^d + h + j | k_i^d + h - 1) - \hat{x}_{i-2}(k_i^d + h + j | k_i^d + h - 1)\|_P^2 \right) \\
 &\leq \sum_{j=0}^{N_p-2} \bar{\lambda}(P) [2(\zeta_i(k_i^d + h + j | k_i^d + h) + \eta_{i-2}(k_i^d + h + j | k_i^d + h)) \cdot \zeta_{i-2}(k_i^d + h + j | k_i^d + h) + \zeta_{i-2}^2(k_i^d + h + j | k_i^d + h)] \tag{A5} \\
 &= \Phi_{i2}
 \end{aligned}$$

Therefore, to sum up $\Delta \bar{J}_i(k_i^d + h) \leq \Phi_{i1} + \Phi_{i2} - \Psi_i$, let $\Phi_{i1} + \Phi_{i2} \leq \sigma_i \Psi_i$, where the trigger parameter $0 < \sigma_i < 1$, then we have $\Phi_{i1} + \Phi_{i2} - \Psi_i \leq (\sigma_i - 1)\Psi_i < 0$. Thus, the trigger condition should be $\Phi_{i1} + \Phi_{i2} > \sigma_i \Psi_i$. □

Appendix B

It can be seen from Lemma 1 that in order to ensure the system ISS, it is first necessary to prove that the performance index function $J(k_i^d)$ of the system is an ISS-Lyapunov function.

For $\forall x_i(k_i^d) \in \mathbb{X}_i$, there is obviously $J(k_i^d) \geq \|x_i(k_i^d)\|_Q^2 \geq \underline{\lambda}(Q) \|x_i(k_i^d)\|^2 \triangleq \chi_1(x_i(k_i^d))$.

Next, we define $J(k_i^d) \triangleq J(k_i^{d,N_p})$, let $J(k_i^{d,1}) = \|x_i(k_i^d)\|_H^2 + \|x_i(k_i^d) - \hat{x}_{i-1}(k_i^d)\|_H^2 + \|x_i(k_i^d) - \hat{x}_{i-2}(k_i^d)\|_H^2 \leq \|x_i(k_i^d)\|_H^2, x_i(k_i^d) \in \mathbb{X}_{if}$, and obtain

$$\begin{aligned}
 J(k_i^{d,N_p-1}) &= J(k_i^{d,N_p}) - \|x_i(k_i^d + N_p - 1 | k_i^d)\|_Q^2 - \|u_i(k_i^d + N_p - 1 | k_i^d)\|_R^2 \\
 &- \|x_i(k_i^d + N_p - 1 | k_i^d) - \hat{x}_{i-1}(k_i^d + N_p - 1 | k_i^d)\|_P^2 - \|x_i(k_i^d + N_p - 1 | k_i^d) - \hat{x}_{i-2}(k_i^d + N_p - 1 | k_i^d)\|_P^2 \\
 &+ \|x_i(k_i^d + N_p - 1 | k_i^d)\|_H^2 - \|x_i(k_i^d + N_p | k_i^d)\|_H^2 + \|x_i(k_i^d + N_p - 1 | k_i^d) - \hat{x}_{i-1}(k_i^d + N_p - 1 | k_i^d)\|_H^2 \tag{A6} \\
 &- \|x_i(k_i^d + N_p | k_i^d) - \hat{x}_{i-1}(k_i^d + N_p | k_i^d)\|_H^2 + \|x_i(k_i^d + N_p - 1 | k_i^d) - \hat{x}_{i-2}(k_i^d + N_p - 1 | k_i^d)\|_H^2 \\
 &- \|x_i(k_i^d + N_p | k_i^d) - \hat{x}_{i-2}(k_i^d + N_p | k_i^d)\|_H^2
 \end{aligned}$$

where

$$\begin{aligned}
 &\|x_i(k_i^d + N_p - 1 | k_i^d)\|_Q^2 + \|u_i(k_i^d + N_p - 1 | k_i^d)\|_R^2 - \|x_i(k_i^d + N_p - 1 | k_i^d)\|_H^2 + \|x_i(k_i^d + N_p | k_i^d)\|_H^2 \tag{A7} \\
 &\leq \left\| \left((A_{i,s} + B_{i,s}K)^T H(A_{i,s} + B_{i,s}K) + Q - H + RK^T K \right) x_i(k_i^d + N_p - 1 | k_i^d) \right\|^2
 \end{aligned}$$

$$\begin{aligned} & \left\| \mathbf{x}_i(k_i^d + N_p - 1 | k_i^d) - \hat{\mathbf{x}}_{i-1}(k_i^d + N_p - 1 | k_i^d) \right\|_P^2 - \left\| \mathbf{x}_i(k_i^d + N_p - 1 | k_i^d) - \hat{\mathbf{x}}_{i-1}(k_i^d + N_p - 1 | k_i^d) \right\|_H^2 \\ & + \left\| \mathbf{x}_i(k_i^d + N_p | k_i^d) - \hat{\mathbf{x}}_{i-1}(k_i^d + N_p | k_i^d) \right\|_H^2 \end{aligned} \quad (\text{A8})$$

$$\begin{aligned} & \leq \left\| \left((\mathbf{A}_{i,s} + \mathbf{B}_{i,s}\mathbf{K})^T \mathbf{H} (\mathbf{A}_{i,s} + \mathbf{B}_{i,s}\mathbf{K}) + \mathbf{P} - \mathbf{H} \right) \mathbf{x}_i(k_i^d + N_p - 1 | k_i^d) - \hat{\mathbf{x}}_{i-1}(k_i^d + N_p - 1 | k_i^d) \right\|^2 \\ & \left\| \mathbf{x}_i(k_i^d + N_p - 1 | k_i^d) - \hat{\mathbf{x}}_{i-2}(k_i^d + N_p - 1 | k_i^d) \right\|_P^2 - \left\| \mathbf{x}_i(k_i^d + N_p - 1 | k_i^d) - \hat{\mathbf{x}}_{i-2}(k_i^d + N_p - 1 | k_i^d) \right\|_H^2 \\ & + \left\| \mathbf{x}_i(k_i^d + N_p | k_i^d) - \hat{\mathbf{x}}_{i-2}(k_i^d + N_p | k_i^d) \right\|_H^2 \end{aligned} \quad (\text{A9})$$

Therefore, (A6) can be further written as:

$$\begin{aligned} J(k_i^{d,N_p-1}) & \geq J(k_i^{d,N_p}) \\ & - \left\| \left((\mathbf{A}_{i,s} + \mathbf{B}_{i,s}\mathbf{K})^T \mathbf{H} (\mathbf{A}_{i,s} + \mathbf{B}_{i,s}\mathbf{K}) + \mathbf{Q} - \mathbf{H} + \mathbf{R}\mathbf{K}^T\mathbf{K} \right) \mathbf{x}_i(k_i^d + N_p - 1 | k_i^d) \right\|^2 \\ & - \left\| \left((\mathbf{A}_{i,s} + \mathbf{B}_{i,s}\mathbf{K})^T \mathbf{H} (\mathbf{A}_{i,s} + \mathbf{B}_{i,s}\mathbf{K}) + \mathbf{P} - \mathbf{H} \right) \mathbf{x}_i(k_i^d + N_p - 1 | k_i^d) - \hat{\mathbf{x}}_{i-1}(k_i^d + N_p - 1 | k_i^d) \right\|^2 \\ & - \left\| \left((\mathbf{A}_{i,s} + \mathbf{B}_{i,s}\mathbf{K})^T \mathbf{H} (\mathbf{A}_{i,s} + \mathbf{B}_{i,s}\mathbf{K}) + \mathbf{P} - \mathbf{H} \right) \mathbf{x}_i(k_i^d + N_p - 1 | k_i^d) - \hat{\mathbf{x}}_{i-2}(k_i^d + N_p - 1 | k_i^d) \right\|^2 \end{aligned} \quad (\text{A10})$$

According to Assumption 1, we know that $J(k_i^{d,N_p-1}) \geq J(k_i^{d,N_p})$. $J(k_i^d) = J(k_i^{d,N_p}) \leq J(k_i^{d,N_p-1}) \leq \dots \leq J(k_i^{d,1}) \leq \left\| \mathbf{x}_i(k_i^d) \right\|_H^2 \leq \bar{\lambda}(\mathbf{H}) \left\| \mathbf{x}_i(k_i^d) \right\|^2 \triangleq \chi_2(\mathbf{x}_i(k_i^d))$ can be obtain. Therefore, the system satisfies Define 3 (condition 1).

By Theorem 1, we know that $J_i(k_i^d + 1) - J_i(k_i^d) \leq \Phi_{i1} + \Phi_{i2} - \Psi_i$, according to (31), we can obtain

$$\begin{aligned} \Phi_{i1} + \Phi_{i2} & \leq (N_p - 1) \left\{ \bar{\lambda}(\mathbf{P}) [4\eta_i(k_i^d) \cdot \bar{\xi}_i(k_i^d) + \bar{\xi}_i^2(k_i^d)] + (N_p - 1) \left\{ \bar{\lambda}(\mathbf{P}) [4\eta_i(k_i^d) \cdot \bar{\xi}_i(k_i^d) + \bar{\xi}_i^2(k_i^d)] \right\} \right. \\ & = 2(N_p - 1) \bar{\lambda}(\mathbf{P}) [4\eta_i(k_i^d) \cdot \bar{\xi}_i(k_i^d) + \bar{\xi}_i^2(k_i^d)] \triangleq \omega(\bar{\xi}_i(k_i^d)) \end{aligned} \quad (\text{A11})$$

$$\Psi_i \geq \left\| \mathbf{x}_i(k_i^d) \right\|_Q^2 \geq \underline{\lambda}(\mathbf{Q}) \left\| \mathbf{x}_i(k_i^d) \right\|^2 \triangleq \chi_1(\mathbf{x}_i(k_i^d)) \quad (\text{A12})$$

Therefore, $J_i(k_i^d + 1) - J_i(k_i^d) \leq -\chi_1(\mathbf{x}_i(k_i^d)) + \omega(\bar{\xi}_i(k_i^d))$, the system satisfies the Define 3 (condition 2).

In summary, the performance index function $J(k_i^d)$ of the system is an ISS-Lyapunov function, and the system is ISS by Lemma 1. \square

References

1. Meo, C.D.; Vaio, M.D.; Flammini, F.; Nardone, R.; Santini, S.; Vittorini, V. ERTMS/ETCS Virtual Coupling: Proof of Concept and Numerical Analysis. *IEEE Trans. Intell. Transp. Syst.* **2020**, *21*, 2545–2556. [\[CrossRef\]](#)
2. Flammini, F.; Marrone, S.; Nardone, R.; Petrillo, A.; Santini, S.; Vittorini, V. Towards Railway Virtual Coupling. In Proceedings of the 2018 IEEE International Conference on Electrical Systems for Aircraft, Railway, Ship Propulsion and Road Vehicles & International Transportation Electrification Conference (ESARS-ITEC), Nottingham, UK, 7–9 November 2018; pp. 1–6.
3. Su, S.; Liu, W.T.; Zhu, Q.Y.; Li, R.Q.; Tang, T.; Lv, J.D. A cooperative collision-avoidance control methodology for virtual coupling trains. *Accid. Anal. Prev.* **2022**, *173*, 106703. [\[CrossRef\]](#)
4. Xun, J.; Li, Y.; Liu, R.; Li, Y.; Liu, Y. A Survey on Control Methods for Virtual Coupling in Railway Operation. *IEEE Open J. Intell. Transp. Syst.* **2022**, *3*, 838–855. [\[CrossRef\]](#)
5. Wu, Q.; Ge, X.; Han, Q.-L.; Liu, Y. Railway Virtual Coupling: A Survey of Emerging Control Techniques. *IEEE Trans. Intell. Veh.* **2023**, *8*, 3239–3255. [\[CrossRef\]](#)
6. Liu, Y.; Ou, D.; Yang, Y.; Dong, D. A Method for Maintaining Virtually Coupled States of Train Convoys. *Proc. Inst. Mech. Eng. Part F J. Rail Rapid Transit* **2023**, *237*, 243–252. [\[CrossRef\]](#)
7. Wang, X.; Hu, M.; Wang, H.; Dong, H.; Ying, Z. Formation Control for Virtual Coupling Trains with Parametric Uncertainty and Unknown Disturbances. *IEEE Trans. Circuits Syst. II Exp. Briefs* **2023**, *70*, 3429–3433.
8. Wang, D.; Cao, Y. Adaptive Cruise Control of Virtual Coupled Trains Based on Sliding Mode. *J. Phys. Conf. Ser.* **2022**, *2224*, 012109. [\[CrossRef\]](#)

9. Wang, H.; Zhao, Q.; Lin, S.; Cui, D.; Luo, C.; Zhu, L.; Wang, X.; Tang, T. A Reinforcement Learning Empowered Cooperative Control Approach for IIoT-Based Virtually Coupled Train Sets. *IEEE Trans. Ind. Informat.* **2021**, *17*, 4935–4945. [[CrossRef](#)]
10. Felez, J.; Kim, Y.; Borrelli, F. A Model Predictive Control Approach for Virtual Coupling in Railways. *IEEE Trans. Intell. Transp. Syst.* **2019**, *20*, 2728–2739. [[CrossRef](#)]
11. Chen, M.; Xun, J.; Liu, Y. A Coordinated Collision Mitigation Approach for Virtual Coupling Trains by Using Model Predictive Control. In Proceedings of the 2020 IEEE 23rd International Conference on Intelligent Transportation Systems (ITSC), Rhodes, Greece, 20–23 September 2020.
12. Su, S.; She, J.; Li, K.; Wang, X.; Zhou, Y. A Nonlinear Safety Equilibrium Spacing-Based Model Predictive Control for Virtually Coupled Train Set Over Gradient Terrains. *IEEE Trans. Transport. Electrific.* **2022**, *8*, 2810–2824. [[CrossRef](#)]
13. Schwenzer, M.; Ay, M.; Bergs, T.; Abel, D. Review on model predictive control: An engineering perspective. *Int. J. Adv. Manuf. Technol.* **2021**, *117*, 1327–1349. [[CrossRef](#)]
14. Xun, J.; Yin, J.; Liu, R.; Liu, F.; Zhou, Y.; Tang, T. Cooperative control of high-speed trains for headway regulation: A self-triggered model predictive control based approach. *Transp. Res. Part C Emerg. Technol.* **2019**, *102*, 106–120. [[CrossRef](#)]
15. Liu, Y.; Liu, R.; Wei, C.; Xun, J.; Tang, T. Distributed Model Predictive Control Strategy for Constrained High-Speed Virtually Coupled Train Set. *IEEE Trans. Veh. Technol.* **2022**, *71*, 171–183. [[CrossRef](#)]
16. Liu, Y.; Zhou, Y.; Su, S.; Xun, J.; Tang, T. Control strategy for stable formation of high-speed virtually coupled trains with disturbances and delays. *Comput. Aided Civ. Inf.* **2023**, *38*, 621–639. [[CrossRef](#)]
17. Zheng, Y.; Li, S.E.; Li, K.; Borrelli, F.; Hedrick, J.K. Distributed Model Predictive Control for Heterogeneous Vehicle Platoons Under Unidirectional Topologies. *IEEE Trans. Control Syst. Technol.* **2017**, *25*, 899–910. [[CrossRef](#)]
18. Zhan, J.; Chen, L.; Chen, Y. Distributed Model Predictive Control of Heterogeneous Vehicle Platoons with Guaranteed String Stability. In Proceedings of the 2021 China Automation Congress (CAC), Beijing, China, 22–24 October 2021; pp. 2086–2091.
19. Huang, D.; Li, H.; Li, X. Formation of Generic UAVs-USVs System Under Distributed Model Predictive Control Scheme. *IEEE Trans. Circuits Syst. II Exp. Briefs* **2020**, *67*, 3123–3127. [[CrossRef](#)]
20. Chen, Q.; Jin, Y.; Wang, T.; Wang, Y.; Yan, T.; Long, Y. UAV Formation Control Under Communication Constraints Based on Distributed Model Predictive Control. *IEEE Access* **2022**, *10*, 126494–126507. [[CrossRef](#)]
21. Zhang, J.; Zhang, H.; Sun, S.; Gao, Z. Leader-follower consensus control for linear multi-agent systems by fully distributed edge-event-triggered adaptive strategies. *Inf. Sci.* **2021**, *555*, 314–338. [[CrossRef](#)]
22. Deng, C.; Wen, C.; Huang, J.; Zhang, X.-M.; Zou, Y. Distributed Observer-Based Cooperative Control Approach for Uncertain Nonlinear MASs Under Event-Triggered Communication. *IEEE Trans. Autom. Control* **2022**, *67*, 2669–2676. [[CrossRef](#)]
23. Zhang, X.; Liu, X.; Wang, P. Distributed Fixed-Time Secondary Control for MTDC Systems Using Event-Triggered Communication Scheme. *Processes* **2023**, *11*, 2329. [[CrossRef](#)]
24. Zou, Y.; Su, X.; Niu, Y. Event-triggered distributed predictive control for the cooperation of multi-agent systems. *IET Control Theory Appl.* **2017**, *11*, 10–16. [[CrossRef](#)]
25. Zhan, J.; Hu, Y.; Li, X. Adaptive event-triggered distributed model predictive control for multi-agent systems. *Syst. Control Lett.* **2019**, *134*, 104531. [[CrossRef](#)]
26. Liu, Y.; Zhou, Y.; Su, S.; Xun, J.; Tang, T. An analytical optimal control approach for virtually coupled high-speed trains with local and string stability. *Transp. Res. Part C Emerg. Technol.* **2021**, *125*, 102886. [[CrossRef](#)]
27. Zou, Y.; Su, X.; Li, S.; Niu, Y.; Li, D. Event-triggered distributed predictive control for asynchronous coordination of multi-agent systems. *Automatica* **2019**, *99*, 92–98. [[CrossRef](#)]
28. Berberich, J.; Koehler, J.; Mueller, M.A.; Allgoewer, F. Data-Driven Model Predictive Control with Stability and Robustness Guarantees. *IEEE Trans. Autom. Control* **2021**, *66*, 1702–1717. [[CrossRef](#)]
29. Hewing, L.; Wabersich, K.P.; Menner, M.; Zeilinger, M.N. Learning-Based Model Predictive Control: Toward Safe Learning in Control. *Annu. Rev. Control Robot. Auton. Syst* **2020**, *3*, 269–296. [[CrossRef](#)]
30. Chen, S.; Wu, Z.; Rincon, D.; Christofides, P.D. Machinelearning-baseddistributed model predictive control of nonlinear processes. *Aiche J.* **2020**, *66*, e17013. [[CrossRef](#)]
31. Zhu, B.; Xia, X. Adaptive Model Predictive Control for Unconstrained Discrete-Time Linear Systems with Parametric Uncertainties. *IEEE Trans. Autom. Control* **2016**, *61*, 3171–3176. [[CrossRef](#)]
32. Lu, X.; Cannon, M. Robust adaptive model predictive control with persistent excitation conditions. *Automatica* **2023**, *152*, 110959. [[CrossRef](#)]
33. Liu, K.; Yang, P.; Wang, R.; Jiao, L.; Li, T.; Zhang, J. Observer-Based Adaptive Fuzzy Finite-Time Attitude Control for Quadrotor UAVs. *IEEE Trans. Aerosp. Electron. Syst.* **2023**, 1–17. [[CrossRef](#)]

Disclaimer/Publisher’s Note: The statements, opinions and data contained in all publications are solely those of the individual author(s) and contributor(s) and not of MDPI and/or the editor(s). MDPI and/or the editor(s) disclaim responsibility for any injury to people or property resulting from any ideas, methods, instructions or products referred to in the content.